OPEN ACCESS
IOP Publishing | Songshan Lake Materials Laboratory
Materials Futures
Mater. Futures 1 (2022) 032301 (21pp)
https://doi.org/10.1088/2752-5724/ac8a63

Topical Review

# Scanning probe microscopy in probing low-dimensional carbon-based nanostructures and nanomaterials

**Chi Zhang, Zewei Yi and Wei Xu***

Interdisciplinary Materials Research Center, College of Materials Science and Engineering, Tongji University, Shanghai 201804, People's Republic of China

E-mail: xuwei@tongji.edu.cn

Received 30 June 2022, revised 3 August 2022
Accepted for publication 17 August 2022
Published 30 August 2022

**Abstract**

Carbon, as an indispensable chemical element on Earth, has diverse covalent bonding ability, which enables construction of extensive pivotal carbon-based structures in multiple scientific fields. The extraordinary physicochemical properties presented by pioneering synthetic carbon allotropes, typically including fullerenes, carbon nanotubes, and graphene, have stimulated broad interest in fabrication of carbon-based nanostructures and nanomaterials. Accurate regulation of topology, size, and shape, as well as controllably embedding target $sp^n$-hybridized carbons in molecular skeletons, is significant for tailoring their structures and consequent properties and requires atomic precision in their preparation. Scanning probe microscopy (SPM), combined with on-surface synthesis strategy, has demonstrated its capabilities in fabrication of various carbon-based nanostructures and nanomaterials with atomic precision, which has long been elusive for conventional solution-phase synthesis due to realistic obstacles in solubility, isolation, purification, etc. More intriguingly, atom manipulation via an SPM tip allows unique access to local production of highly reactive carbon-based nanostructures. In addition, SPM provides topographic information of carbon-based nanostructures as well as their characteristic electronic structures with unprecedented submolecular resolution in real space. In this review, we overview recent exciting progress in the delicate application of SPM in probing low-dimensional carbon-based nanostructures and nanomaterials, which will open an avenue for the exploration and development of elusive and undiscovered carbon-based nanomaterials.

Keywords: scanning probe microscopy, carbon nanostructures, carbon nanomaterials, synthetic carbon allotropes, on-surface synthesis

* Author to whom any correspondence should be addressed.

**Future perspectives**
Scanning probe microscopy (SPM) has significantly facilitated atomically precise synthesis, fine structural characterization, and property measurement of low-dimensional carbon-based nanostructures and nanomaterials. Combined with on-surface synthesis strategy, SPM has been witnessing delicate fabrication and in-depth exploration of a broad range of promising carbon-based nanostructures (including synthetic carbon allotropes) on surfaces, which were considered to be elusive for conventional solution-phase synthesis. We highlight recent remarkable advances in the application of SPM techniques in probing carbon-based nanostructures and nanomaterials mainly from the aspects of on-surface synthesis, topographic characterization, and electronic structure detection. This atomic-level investigation and understanding will shed light on further full exploitation of carbon-based electronics and spintronics.

## 1. Introduction

Carbon is an indispensable and ubiquitous chemical element on Earth. All life is dependent on carbon element and inevitably involved in the chemistry of carbon. Carbon atoms generally form bonds with different types of hybridization (i.e. $sp^3$, $sp^2$, and sp hybridization), leading to various bond angles and geometries and accordingly, structural diversity. The diverse covalent bonding ability of carbon element gives rise to extensive pivotal carbon-based structures in multiple scientific fields, ranging from chemistry and materials to biology and pharmacy. Among others, organic chemistry is entirely based on carbon element, which constructs carbon-based compounds via bonding to a wide variety of chemical elements. For instance, hydrocarbon is a class of chemical compounds made up of carbon and hydrogen exclusively, including alkanes, alkenes, alkynes, and aromatic hydrocarbons as representative ones. Moreover, the diverse bonding ability of carbon also enables itself to bond together constructing carbon allotropes, such as diamond (comprising $sp^3$-hybridized carbon atoms, shortened as $C(sp^3)$) and graphite (with $C(sp^2)$) in nature [1]. The emergence of zero-dimensional (0D) fullerenes (containing $C(sp^2)$) [2] further brings the new era of carbon allotropes and has stimulated intense interest and in-depth exploration of synthetic carbon allotropes thereafter [1], typically including one-dimensional (1D) carbon nanotubes [3] and two-dimensional (2D) graphene [4]. These $C(sp^2)$-containing synthetic carbon allotropes, featured with delocalization of $\pi$-electrons, have been demonstrated to share extraordinary physicochemical properties (such as outstanding electrical transport and redox activity [1, 5]) while having their respective unique properties, which are directly determined by their chemical structures (topology, size, shape, etc). In addition, depending on the different types of $sp^n$ ($n = 1$, 2, 3) hybridization involved in the synthetic carbon allotropes, the corresponding structures and properties are distinct. Therefore, controllably embedding the target $C(sp^n)$ in the molecular skeletons, along with accurate regulation of topology, size, and shape, is significant for tailoring the structures as well as outcoming physicochemical properties, inspiring a broad range of synthetic carbon allotropes and other carbon-based materials. A well-known example is the 2D graphyne family (including graphyne, graphdiyne, and graphyne-*n*) [6–8] with acetylenic (sp) linkages embedded in graphene ($sp^2$) structures, which is promising for nanoelectronics, photovoltaics, and catalysis. Another interesting example is the 1D carbyne [9], which features ideal finite sp-hybridized carbon chain and is theoretically predicted to be a mechanically strong and electronically prominent material [10, 11].

Despite lots of remarkable achievements in the discovery, prediction, and preparation of carbon-based materials, many of them are still in their very early infancy. It has long been of great challenge to synthesize or prepare uniform monodisperse carbon-based structures and materials [1] by traditional solution-phase synthesis. Difficulties lie in many key processes, such as dissolution in solvents, stabilization as dispersions, and purification [5], which are also closely related to the high reaction activity and poor reaction selectivity of unsaturated carbon skeletons (C(sp) skeletons, in particular). Consequently, it turns out to be elusive to precisely fabricate such carbon-based structures and materials, which is a realistic obstacle for their detailed structural characterization, property measurement, and further full exploitation (e.g. application in devices). On-surface synthesis strategy, as an emerging synthetic strategy generally combined with scanning probe microscopy (SPM) techniques, takes full advantage of the templating and catalytic effects provided by the substrates involved [12–15] and has proved its capabilities in synthesizing numerous carbon-based nanostructures and nanomaterials with atomic precision. Monodispersed carbon-based nanostructures, such as isolated 0D motifs, 1D chains, and 2D single layers, are accessible based on this versatile protocol, which overcomes the limitations of conventional synthetic methods, and more significantly, enables novel or unexpected reaction pathways and products [15–19]. Standing on the shoulder of this strategy, SPM techniques [20], which are mainly based on scanning tunneling microscopy (STM) and atomic force microscopy (AFM), provide easy access to topographic information of carbon-based nanostructures in real space as well as their characteristic electronic structures on surfaces (cf figure 1). More intriguingly, atom manipulation [21] by applying controlled voltage pulses from an SPM tip to the nanostructures beneath is able to trigger chemical reactions locally, producing unique carbon-based nanostructures [22, 23] with extreme reactivity which are generally considered to be inaccessible (figure 1). These powerful aspects have been pushing the development of many elusive and undiscovered low-dimensional carbon allotropes and relevant hydrocarbons with embedding of various $sp^n$-hybridized carbons.

In this review, we summarize recent exciting progress in the delicate application of SPM in probing low-dimensional carbon-based nanostructures and nanomaterials mainly from the aspects of on-surface synthesis, topographic characterization, and electronic structure detection. Some typical carbon-based nanostructures and nanomaterials are discussed, which cover different dimensions ranging from 0D to 2D (see figure 1 for more details), and the main focus is the 0D

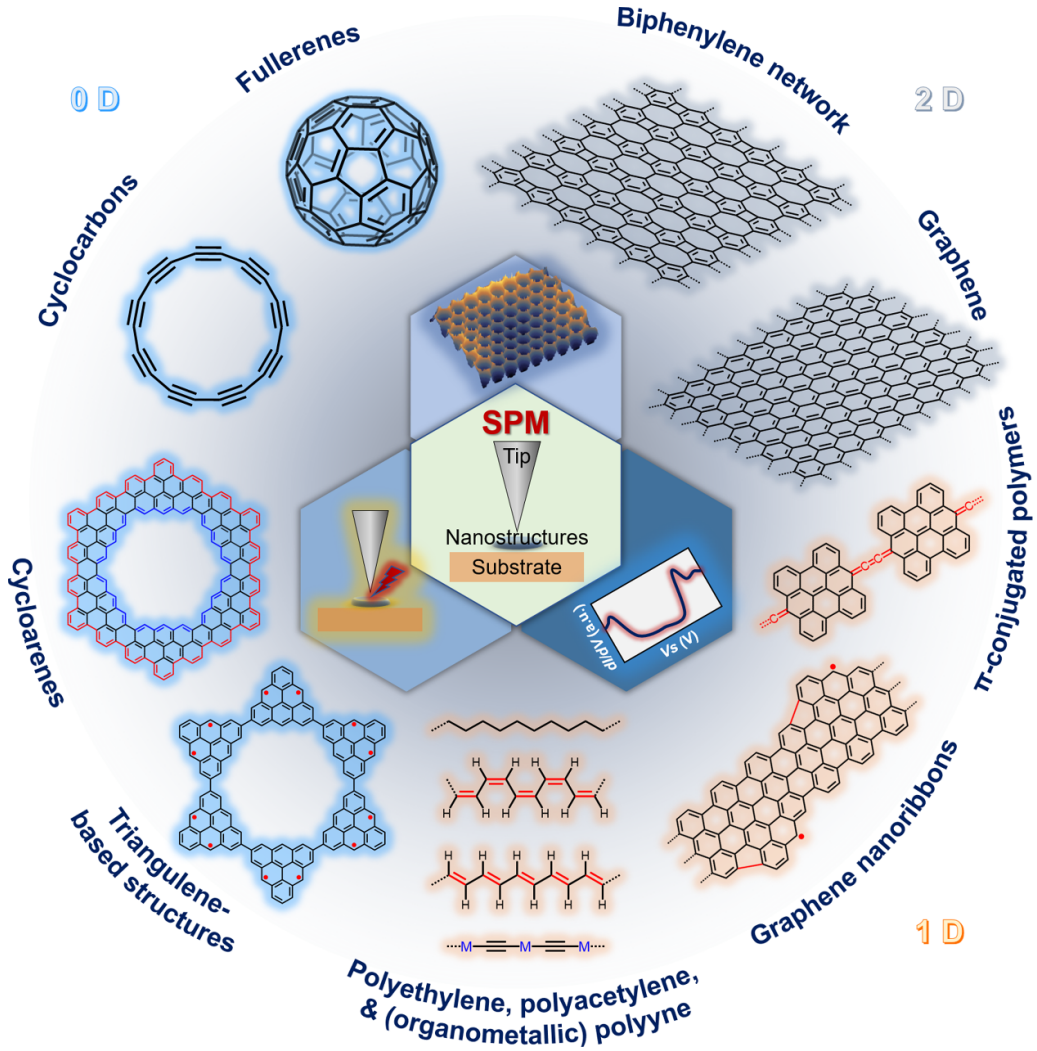


**Figure 1.** Schematic illustration showing the application of SPM techniques in the exploration of carbon-based nanostructures and nanomaterials on surfaces.

and 1D ones as elementary components or segments for the extended 2D ones. In the 0D carbon-based nanostructures and nanomaterials, carbon allotropes involving $sp^2$-hybridized fullerenes and pure sp-hybridized cyclo[*n*]carbons are introduced as a starting point with limited lateral sizes. As an extension, a series of C($sp^2$)-constructed nanographenes fabricated by virtue of on-surface synthesis strategy are displayed, including small rectangular graphene segments, cycloarenes, segments embedded with non-benzenoid n-membered rings, and more complicated graphene-related oligomers and macrocycles (such as triangulene-based structures). Regarding 1D structures, we describe the transformations and reactions involved in the synthesis of polyethylene (PE) (C($sp^3$)), polyacetylene (PA) (C($sp^2$)), and (organometallic) polyyne (C(sp)) and their skeleton visualization and electronic property measurement. In addition, studies on graphene nanoribbons (GNRs) (C($sp^2$)) and other $\pi$-conjugated polymer chains (with dominantly C($sp^2$) and integration of C(sp)) are summarized. By extending the lateral width from 1D structures, several typical 2D carbon-based nanostructures and nanomaterials that are highly related to graphene, have been achieved and are also briefly reviewed herein. Moreover, recent advances in tip-functionalized STM (also known as bond-resolved STM (BRSTM)) and non-contact AFM (nc-AFM) offer possibilities of identification and assignment of unknown structures with submolecular or even atomic resolution, which also enable bond-order analysis of carbon-based nanostructures. Additionally, scanning tunneling spectroscopy (STS) provides complementary spectroscopic information, including but not limited to determination of band gaps and spin configurations and visualization of molecular frontier orbitals, which describe semi-conducting and metallic features of carbon-based nanostructures and nanomaterials as well as carbon-based magnetism and spintronics. These important applications of SPM techniques are also discussed in this review, which are expected to provide a brief overview of the connection between SPM techniques and carbon-based materials.

## 2. 0D carbon-based nanostructures and nanomaterials

The discovery of $C_{60}$ (buckminsterfullerene, with all carbon atoms in $sp^2$ hybridization) in 1985 [2] opened the era of carbon allotropes and has stimulated intense interest and in-depth exploration of synthetic carbon allotropes [1]. Thereafter, the successful fabrication of 1D carbon nanotubes [3] and 2D graphene [4] further enriched the family of $sp^2$-hybridized synthetic carbon allotropes, and brought about new opportunities and challenges for the development of many elusive and undiscovered allotropes as well as related hydrocarbons with embedding of various $sp^n$-hybridized carbons. The combination of on-surface synthesis strategy and SPM techniques has been demonstrated to be versatile in breaking through numerous limitations of conventional solution-phase synthesis (e.g. poor stability, difficulties in purification) and facilitating unique on-surface reactions. In this part, we focus on some 0D carbon-based nanostructures and nanomaterials which have been precisely synthesized and finely characterized by virtue of on-surface synthesis strategy and SPM techniques.

### *2.1. Fullerenes, cyclocarbons, and nanographenes in small size*

In 2008, Otero *et al* reported the synthesis of fullerenes (i.e. $C_{60}$ and triazafullerene $C_{57}N_3$) from aromatic precursors on Pt (111) by a surface-catalyzed cyclodehydrogenation process (figure 2(a)) [24], which provided an amazing example revealing the great potentials of surface-facilitated reactions. Since then, fullerene-related studies have attracted great interest, such as the synthesis of higher fullerenes ($C_{84}$) and buckybowls [25], the reaction selectivity between triazafullerene $C_{57}N_3$ and 2D polyaromatic architectures [26], the sequential synthesis of nanohelicene, nanographene and nanodome [27], the fabrication and mechanistic exploration of graphene quantum dots from $C_{60}$ via a metal-catalyzed cage-opening process [28], etc. Due to the relatively large apparent height of fullerenes (in the range of 0.3–0.4 nm) on surfaces [24] compared to planar molecules, they appeared as bright round protrusions in STM images [24]. Such an obvious corrugation of surface structures along $z$-axis leads to the great challenge in the intramolecular structure characterization. As well-demonstrated by Gross *et al* [29], nc-AFM based on a qPlus sensor [30], which is further functionalized with a single CO molecule at the tip apex, enables unprecedented atomic resolution by probing short-range chemical forces involved. With such a CO-terminated tip, nc-AFM could also be applied to discriminate different bond orders involved in the carbon-based nanostructures (such as fullerenes), which were demonstrated to be closely related to the electron density in bonds [31]. Interestingly, due to the tilting of the CO molecule positioned at the tip apex, only a hexagonal tile was exhibited in the nc-AFM images of fullerenes, and the atomic contrast stemmed from Pauli repulsion. Thus, it is generally difficult yet highly desirable to develop new methodologies to characterize 3D or nonplanar molecular skeletons as well as surface structures. Remarkably, Moreno *et al* developed a multipass method to image such nonplanar molecules (including $C_{60}$) with intramolecular resolution based on the application of AFM with silicon cantilevers as force sensors (figure 2(b)) [32]. Two consecutive line scans were conducted as schematically shown in the top left panel of figure 2(b). The first line scan of a single $C_{60}$ adsorbed on a (101) anatase surface (top right) provided the topography resolved as a bright dot, while the $\Delta f$ and $\Delta f_2$ images (bottom) obtained during the second line scan (with an offset along $z$-axis of $-0.21$ nm in this case) revealed the skeletal features comprising hexagonal and pentagonal rings. This intramolecular bond-resolved capability indicates a promising way to study 3D systems such as nonplanar carbon nanostructures, which would also be an important supplement to that acquired from CO-functionalization.

In 2019, Kaiser *et al*, for the first time, fabricated an isolated cyclo[18]carbon ($C_{18}$, an sp-hybridized molecular carbon allotrope) by atom manipulation on a $C_{24}O_6$ molecule adsorbed on bilayer NaCl/Cu(111) (figure 2(c)) [22]. By applying voltage pulses from an STM/AFM tip, the CO moieties were sequentially cleaved, resulting in the generation of $C_{18}$ with a yield of 13%. The nc-AFM images recorded at different tip offsets $\Delta z$ with respect to the setpoint clearly displayed the differences in bond order, which helped to experimentally discriminate between the two possible chemical structures of $C_{18}$ (i.e. polyynic and cumulenic forms). Consequently, a nine-fold symmetry was directly observed from the AFM contrast, and a polyynic structure was revealed. Apart from the decarbonylation pathway, the authors further demonstrated that an alternative strategy, dehalogenation from a $C_{18}Br_6$ precursor via voltage pulses, provided a higher yield of 64% [33]. These results open up the possibility to synthesize carbon-rich structures with high reactivity followed by structural characterization based on SPM techniques, which would otherwise be inaccessible by conventional synthetic methods due to the difficulties not only in synthesis but also in isolation.

Aside from C($sp^2$)-containing fullerenes, nanographenes, which are well-defined graphene segments and extended polycyclic aromatic hydrocarbons (PAHs) [34], have great potential in molecular electronics and have been a topic of broad interest. Experimental and theoretical investigations have revealed a close correlation between electronic properties and various edge geometries [35] and sizes [36] of nanographenes. A series of progress concerning nanographenes based on the application of STM was reviewed by Müllen and Rabe [34], and they described the structures and electronic properties (e.g. rectification) probed by STM/STS. Recent years have witnessed the booming on-surface synthesis strategy for nanographenes as well as the development of real-space fine characterization. Among all the synthetic strategies, reaction pathways via C–H [37] and/or C–X [38] (X: halogen) activation have shown their superiority in producing products with a high reaction selectivity. Based on the surface-assisted C–H activation, periacenes, such as peripentacene [39] and oxygen–boron–oxygen-doped perihexacene [40], were synthesized via

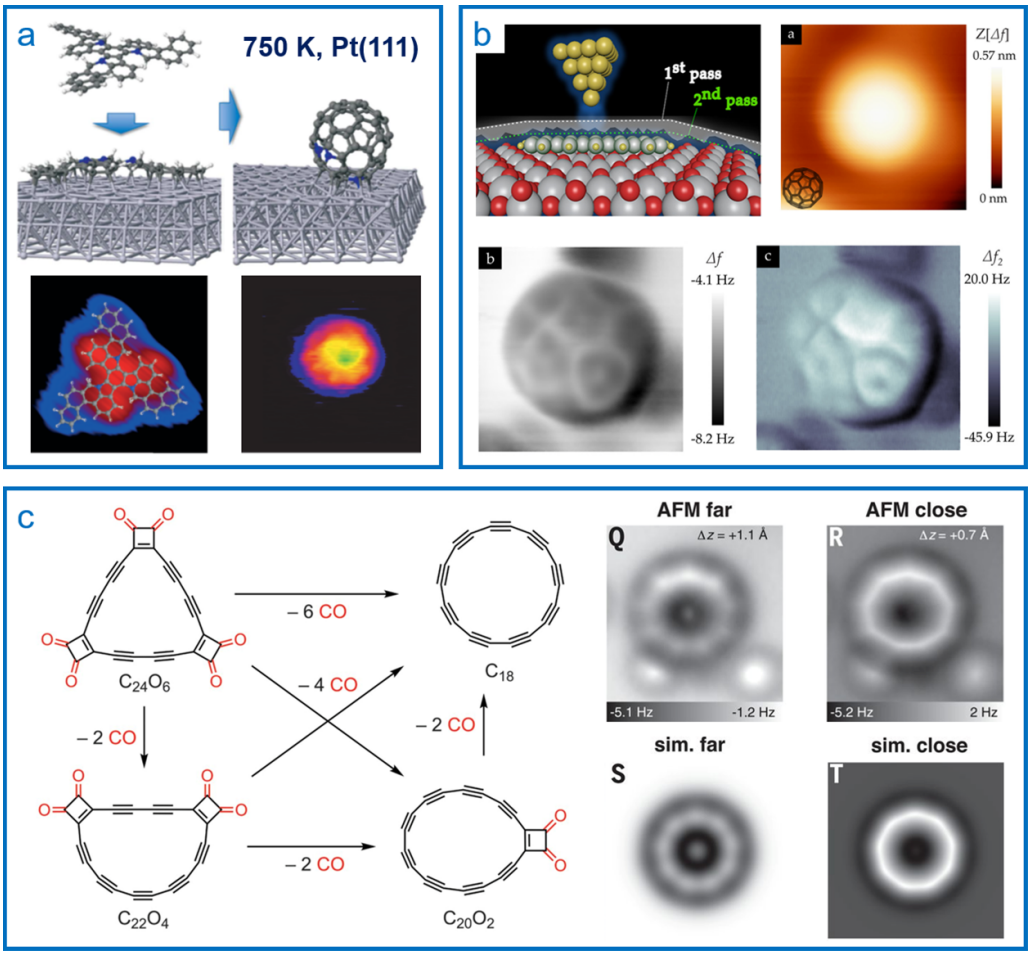


**Figure 2.** On-surface synthesis and characterization of 0D nanostructures, including fullerenes and cyclo[18]carbons. (a) Synthesis of triazafullerene $C_{57}N_3$ on Pt(111) and corresponding STM characterization. Reproduced from [24], with permission from Springer Nature. (b) AFM characterization of $C_{60}$ on a (101) anatase surface with intramolecular resolution using a multipass method. Reprinted with permission from [32]. Copyright (2015) American Chemical Society. (c) *In-situ* generation of cyclo[18]carbon by atom manipulation and subsequent structural characterization. From [22]. Reprinted with permission from AAAS.

cyclodehydrogenation reactions on Au(111). In addition, a rationally designed synthetic route via the dehydrogenative coupling of adjacent methyl groups led to the ultrahigh-yield fabrication of circumcoronene on Cu(111) [41]. Furthermore, by a combination of STM/nc-AFM imaging and density functional theory (DFT) calculations, Zhong *et al* reported the on-surface synthesis of dibenzoperihexacenes (with and without *tert*-butyl (*t*Bu) groups) and dibenzoperioctacene (with *t*Bu groups, as shown in figure 3(a)) on Au(111) starting from tetranaphthyl-*p*-terphenyl and tetra-anthryl-*p*-terphenyl precursors, respectively [42]. They clearly revealed the differences between reactions occurring on surfaces and those in solution [43] in regioselectivity, reaction pathways, and products. Interestingly, the energy gaps were measured to be 2.1 eV and 1.3 eV for dibenzoperihexacenes and dibenzoperioctacene on Au(111) by STS, respectively, indicating the influence of the nanographene core size in the electronic properties. The critical dependence of electronic structure on the topologies was also systematically demonstrated by Fasel *et al* in the open-shell nanographene systems [38, 44–46], which host unpaired electrons and remain challenging for solution synthesis. Open-shell nanographenes were generated on surfaces, and bond topologies [44] and topological defects [38] involving non-benzenoid rings were demonstrated to be capable of inducing magnetism by STM/STS. Moreover, it is worthy to remark that in the system of Clar's goblet ($C_{38}H_{18}$) [45], a combination of STM (with a magnetic field) and spin excitation spectroscopy directly provided electronic and magnetic characterization and revealed the unconventional magnetism resulting from the topological frustration, which would be significant for carbon-based spintronics. Recently, rhombus-shaped nanographenes with zigzag peripheries including [4]- and [5]-rhombenes [46] were synthesized, and a magnetic spin singlet ground state emerged with increasing nanographene size.

In addition, a special type of PAHs featuring defined central cavities, that is cycloarenes, are regarded as models for porous graphene (i.e. unique nanographenes) and have been intriguing researchers due to their singular molecular and electronic structures [47]. As restricted by the challenges in synthesizing such macrocyclic molecular systems, the precise synthesis and in-depth characterization were quite

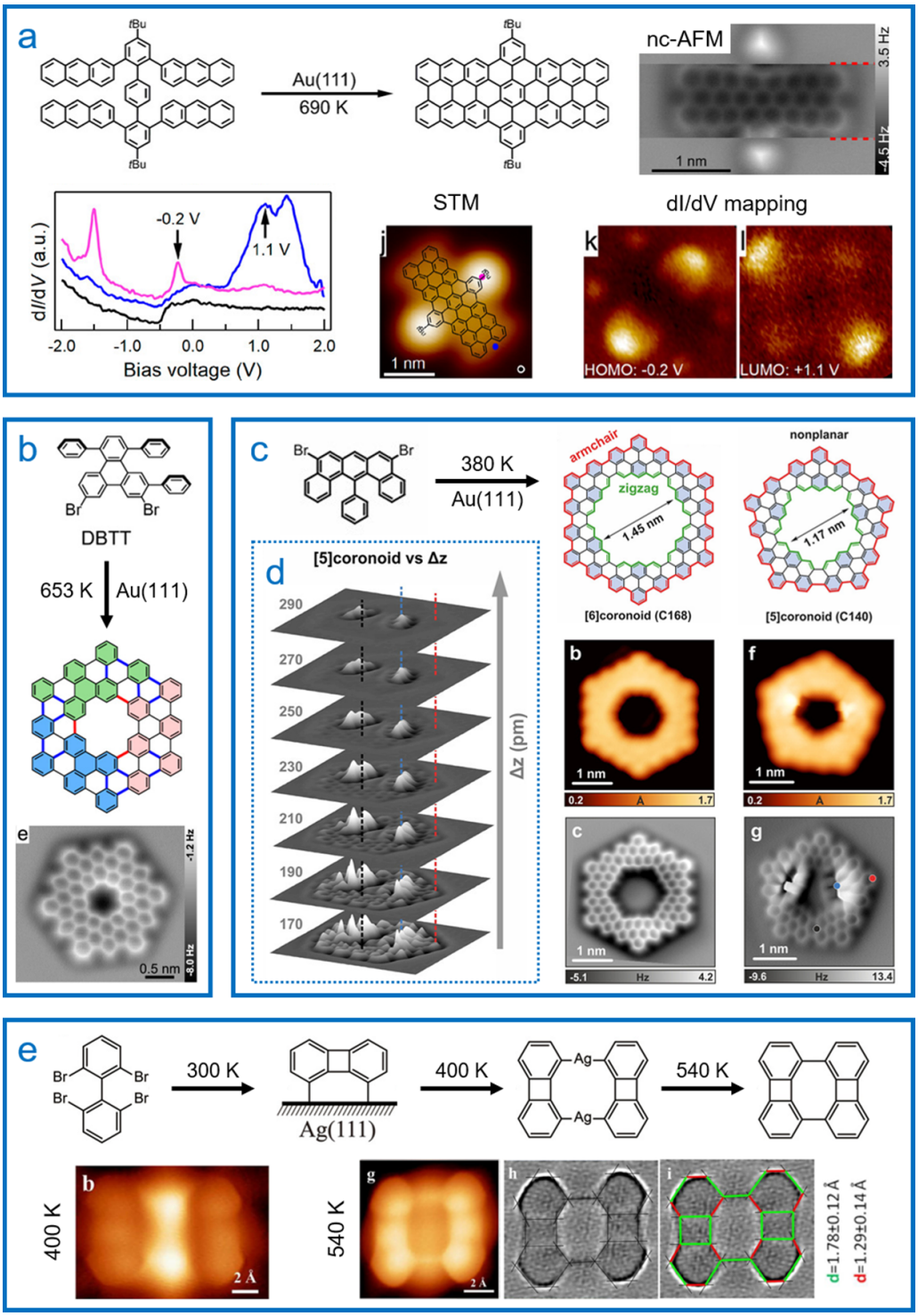


**Figure 3.** On-surface synthesis and characterization of 0D nanographenes in small sizes. (a) Synthesis and STM/STS/nc-AFM characterization of dibenzoperioctacenes on Au(111). Reproduced from [42]. CC BY 4.0. (b) Fabrication of a C108 cycloarene on Au(111). Reprinted with permission from [52]. Copyright (2020) American Chemical Society. (c) Synthesis and characterization of [6]- and [5]coronoids on Au(111). (d) Z-dependent nc-AFM images of a [5]coronoid. (c), (d) Reproduced from [53]. CC BY 4.0. (e) Reaction process and intermediate states detected in the formation of biphenylene dimers on Ag(111). Reprinted with permission from [55]. Copyright (2022) American Chemical Society.

elusive until the successful fabrication of kekulene through a double Diels–Alder reaction and nc-AFM-based structural characterization [48] by Pozo *et al*. Thereafter, taking the advantage of surface-facilitated cyclodehydrogenation reactions [42, 49–51], Fan *et al* demonstrated the on-surface synthesis protocol of a double-stranded hexagonal cycloarene, i.e. a C108 cycloarene, by applying a dibrominated precursor on Au(111) (figure 3(b)) [52]. The nc-AFM characterization

unambiguously visualized the armchair edges at both inner and outer sides. In addition to such an edge geometry, remarkably, C168 and C140 cycloarenes (namely [6]- and [5]coronoids) featuring inner zigzag edges and outer armchair edges were later synthesized on Au(111) (figure 3(c)) [53] by Di Giovannantonio *et al*. The well-designed dibrominated U-shaped precursor (cf figure 3(c)) underwent dehalogenative coupling and subsequent cyclodehydrogenation, which was similar to the situation in the previous case [52], leading to the fabrication of planar [6]coronoids and strain-driven nonplanar [5]coronoids as elucidated by the ultra-high-resolution STM/nc-AFM images shown below (figure 3(c)). The tip-height (z)-dependent nc-AFM images shown in figure 3(d) recorded the frequency shift when the CO-tip approached a [5]coronoid at different $\Delta z$ values with respect to the setpoint, and a height difference of $180 \pm 10$ pm was thus extracted. The d$I$/d$V$ spectra directly detected the HOMO-LUMO (shortened for highest occupied molecular orbital to lowest unoccupied molecular orbital) gaps, that is ∼2.97 eV for the C108 cycloarene on Au(111) [52], and ∼2.2 eV and ∼2.5 eV for [6]- and [5]coronoids on Au(111) [53], respectively. Besides, extended from the single nanopore structure described above, a well-designed triple-porous C78 nanographene with a nonplanar conformation was also realized on Au(111) with an electronic gap of ∼3.0 eV [54], which broadened the diversity of nanographenes.

Moreover, due to the surface confinement and facilitation, some unique 0D carbon-based nanostructures, such as those embedded with non-benzenoid *n*-membered rings, have been demonstrated to be accessible by on-surface reactions. Simultaneously, SPM techniques play a significant role in the detection of intermediates and revelation of reaction pathways [55, 56], visualization of bond structures and topographies [55, 57–64], characterization of electronic properties [58, 59, 65], tip-induced structural transformations [59, 66], etc. Notably, Zeng *et al* applied a tetrabromobiphenyl molecular precursor with dibromo groups functionalized at the bay region of both sides and selectively fabricated biphenylene dimers containing four-, six-, and eight-membered rings on Ag(111) (figure 3(e)) [55]. Intriguingly, a unique reaction pathway was determined based on STM and synchrotron radiation photoemission spectroscopy. It involved a key step of intramolecular annulation, resulting in a surface-stabilized biradical biphenylene monomer, which was followed by the generation of an organometallic intermediate state and a biphenylene dimer (lower panels of figure 3(e)) with the increasing temperature. A detailed STM-based structural detection and analysis suggested antiaromaticities for four- and eight-membered rings. The controlled integration of *n*-membered rings and attendant novel properties shown in the above studies indicates a bright prospect in the subtle regulation of nanographenes alternatively.

### 2.2. Nanographene-related oligomers and macrocycles

In addition to the above-mentioned nanographenes in relatively small sizes, some larger nanographene-related structures have also been successfully fabricated on surfaces. Although their solution synthesis usually encounters size and shape limitations, the on-surface synthesis protocol takes full advantage of key molecular building blocks stemming from solution chemistry (namely, molecular precursors) as well as surface-facilitated chemical reactions, and thus enables a precise bottom-up preparation of these covalently coupled carbon nanostructures. In this regard, a cascade of well-predesigned on-surface intermolecular and intramolecular reactions is a reaction strategy of choice, which generally involves Ullmann-type coupling reactions (via C–X activation and C–C coupling) and cyclodehydrogenation reactions (as a surface-assisted planarization process via C–H activation).

An amazing example of such exquisite design was shown in figures 4(a)–(c) [67], as reported by Hieulle *et al*. A 12-ring dibromo polycyclic aromatic compound ($C_{62}H_{38}Br_2$) was applied as the precursor and underwent Ullmann coupling and subsequent cyclodehydrogenation processes on Au(111), forming a trimer-like structure. Owing to the high steric hinderance (which is often the case for cyclodehydrogenation steps [42, 49, 50]) at the conjoined cove regions (indicated by red arrows in the inset of figure 4(a)), cyclodehydrogenation was spontaneously triggered, and planar nanographenes ($C_{186}H_{60}$) with the incorporation of six azulene moieties was consequently synthesized (figures 4(a) and (b)). Among all the trimers, a C3-symmetric one was shown in figure 4(b), and the intramolecular skeletal structure was clearly resolved from a constant-height d$I$/d$V$ map using a CO-functionalized STM tip. About 21 rings (including two azulene moieties) were resolved for each blade with a large [18]annulene one located at the center of the trimer, indicating that the trimer was composed of 64 carbon rings. A highly localized electronic state at the [18]annulene pore was visualized by d$I$/d$V$ mapping at an energy of 2.4 V (figure 4(c)), displaying a special electronic state related to super-atom molecular orbitals. Besides, carbon nanostructures with regularly fused azulenes were further synthesized through a skeletal rearrangement by Hou *et al* [68].

Triangulene nanographenes, known as Clar's hydrocarbon, serve as appealing model systems for the exploration of carbon-based magnetism and spintronics, and thus have been extensively studied on surfaces in the recent five years, typically including [*n*]triangulenes and trangulene-based nanographenes [69] (e.g. Clar's goblet [45], $C_{38}H_{18}$, as discussed above). Notably, the extreme reactivity of unsubstituted [*n*]triangulenes originated from their special chemical structures with unpaired electrons brings about a huge challenge in their synthesis. Consequently, the synthesis had long been elusive until the landmark work concerning the generation of [3] triangulene on surface via STM/AFM tip-induced dehydrogenation was reported by Pavliček *et al* [70] in 2017. The subsequent successful synthesis and characterization of [4]-, [5]-, and [7]-triangulenes [71–73] and [7]triangulene quantum ring [74] by SPM-based techniques have greatly expanded the fundamental understanding and further stimulated intensive exploration of triangulene family [69], such as triangulene dimer [75], trimer [76], chains [77], and aza-triangulene [78]. Moreover, by subtly combining solution synthesis

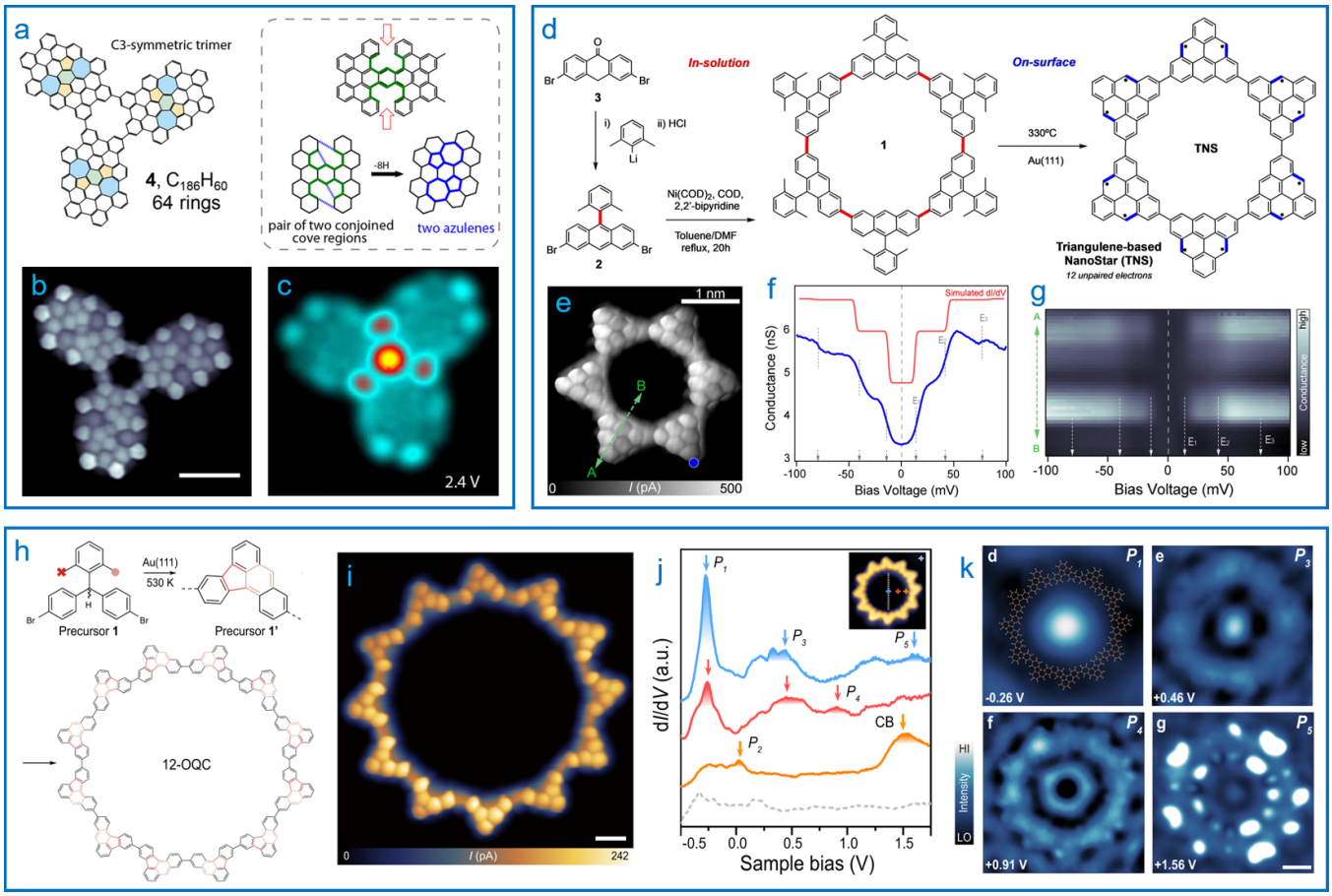


**Figure 4.** On-surface synthesis and characterization of graphene-related oligomers and macrocycles. (a) Chemical structure; (b) constant-height d$I$/d$V$ map characterization with a CO-tip; and (c) constant-height d$I$/d$V$ map (at 2.4 V) of nanographenes ($C_{186}H_{60}$) with azulene moieties embedded on Au(111). Scale bar in (b): 1.2 nm. Reprinted with permission from [67]. Copyright (2018) American Chemical Society. (d) Synthetic route and (e) skeletal characterization of a triangulene-based nanostar. (f) d$I$/d$V$ spectra acquired at the edge of a triangulene unit on Au(111) as marked by the blue dot in (e). (g) Stacked d$I$/d$V$ plot along the line AB depicted in (e). (d)–(g) [79] John Wiley & Sons. [© 2021 The Authors. Angewandte Chemie International Edition published by Wiley-VCH GmbH]. (h) Synthesis and (i) skeletal characterization of a covalently linked organic quantum corral on Au(111). Scale bar: 5 Å. (j) d$I$/d$V$ spectra acquired at different sites inside the organic quantum corral on Au(111). (k) d$I$/d$V$ maps characterizing the quantum resonance states trapped inside the organic corral. Scale bar: 1 nm. (h)–(k) Reproduced from [81]. CC BY 4.0.

and one-step on-surface cyclodehydrogenation, Hieulle *et al* reported the synthesis of a triangulene-based nanostar, which was a macrocycle constructed by six [3] triangulenes, and its spin excitations on Au(111) (figures 4(d)–(g)) [79]. It is noteworthy that a cascade of Ullmann coupling and cyclodehydrogenation of compound 2 (cf figure 4(d)) on Au(111) led to the formation of triangulene-based oligomers [77] instead of a nanostar structure. Alternatively, the macrocycle 1 served as the precursor and was directly sublimated onto Au(111) by flash-annealing, followed by a surface-mediated cyclodehydrogenation upon further annealing. The resulting planarized triangulene-based nanostar was confirmed based on the BRSTM image obtained by a CO-terminated STM tip (figure 4(e)). Besides, its spin configuration was probed by the d$I$/d$V$ spectra conducted at the edge of a triangulene unit (marked by the blue dot in figure 4(e)), which indicated bias-symmetric stepped features as a fingerprint of inelastic electron tunneling induced spin excitation (figure 4(f)). The stacked d$I$/d$V$ plot along the line AB displayed the distribution of the inelastic signals, which were localized at the edges and dissipated at the unit center (figure 4(g)). Three steps located at $\pm$14(1) mV, $\pm$42(2) mV, and $\pm$80(2) mV were clearly resolved, presenting a direct evidence for the unique collective spin state for such a triangulene hexamer, which corresponded to the antiferromagnetic ordering of six $S = 1$ sites. Besides, detailed exploration of length-dependent magnetic excitations in triangulene-extended chains and macrocycles was sophisticatedly performed by Mishra *et al* [77], and gapped spin excitations and fractional edge states were directly observed based on the STM/STS. More details and insights into the characterization of spin-polarized electronic properties of graphene nanostructures using SPM techniques have been comprehensively covered by the review paper by Song *et al* [80] and are skipped herein.

Moreover, SPM techniques have also shown the remarkable potential in the bottom-up synthesis of sizeable covalently linked organic quantum corrals and direct visualization of the quantum resonance states residing inside [81] as reported by

Peng *et al* (figures 4(h)–(k)). A perfect 12-unit circular organic ring (with a pore of 3.86 nm in diameter) was prepared following the on-surface synthetic route shown in figure 4(h), along with the formation of chains and ring segments. BRSTM imaging (figure 4(i)) visualized each unit involved, which was made up of one five-membered ring and four six-membered rings resulting from dehydrogenative cyclization. Electronic characterization by d$I$/d$V$ spectra revealed the valence band and conduction band of the organic quantum corral to be located at $-1.05$ eV and $+1.3$ eV with respect to the Fermi level, respectively. The corresponding characteristic frontier orbitals were experimentally visualized by d$I$/d$V$ mapping at these energies, showing a localized strong intensity at the edges. Interestingly, the authors further probed quantum resonance states inside the organic corrals based on d$I$/d$V$ spectra and mapping (figures 4(j) and (k)). Five electronic states (i.e. $P_1$–$P_5$) were detected from the d$I$/d$V$ spectra at different positions with respect to the pore center (figure 4(j)), and the corresponding spatial distribution was probed by mapping showing distinct characteristic features (figure 4(k)). These quantum resonance states were also shown to be related to the topographies of organic corrals, which opened up a new avenue to engineer desired quantum states.

## 3. 1D carbon-based nanostructures and nanomaterials

When the dimension of carbon-based nanostructures extends to 1D, many intriguing nanomaterials emerge with fascinating physicochemical properties and phenomena. In this part, we will mainly focus on 1D carbon-based nanostructures and nanomaterials probed by SPM. Carbon-based chains with negligible widths will be discussed first, which typically include PE, PA, and (organometallic) polyyne. Thereafter, with the increasing width to several atoms, GNRs and other $\pi$-conjugated polymer chains will be introduced herein, which would also be important model systems for the corresponding 2D extended networks.

### 3.1. PE, PA, and (organometallic) polyyne

Alkanes, known as single-bonded saturated hydrocarbons with a molecular formula of $C_nH_{2n+2}$, are generally applied as natural gas (methane and ethane), fuel, and feedstock in chemical production. With each carbon atom in $sp^3$ hybridization forming strong and localized C–C and C–H bonds [82], alkanes are usually considered to be less reactive and are accessible from alkenes ($C_nH_{2n}$) and alkynes ($C_nH_{2n-2}$) by addition reactions with molecular hydrogen. Meanwhile, the selective hydrogenation of alkynes to alkenes without further formation of alkanes has long been an important yet challenging topic in heterogeneous catalysis. The transformation from acetylene ($C_2H_2$) to ethylene ($C_2H_4$) or ethane ($C_2H_6$) has been systematically explored on single-atom alloys (SAAs) and metal substrates using ultrahigh vacuum (UHV) techniques [83, 84] by Trenary *et al* as model systems to monitor such a selective $H_2$ addition process and unravel catalytic mechanisms. In addition, due to the relative inertness and abundance of alkanes, controllable and efficient C–H bond activation in alkanes is of great importance in exploiting alkane resources for fine chemical synthesis [82, 85]. The combination of surface science methodologies and catalysis studies has successfully opened the door to the mechanistic understanding of C–H bond activation at an atomic scale, including catalytically active sites, reaction pathways, reaction intermediates, etc. For example, the dehydrogenation of alkane was investigated by Marcinkowski *et al* on Pt/Cu SAAs [86], revealing the evolution of methyl groups and the promising catalytic role of SAAs in C–H bond activation.

Aside from these great efforts, the transformations and reactions of alkane, PE, and PA have been intriguing in the field of on-surface chemistry. Dated as far back as the early nineties, seminal works on self-assembled alkanes were carried out at the liquid-solid interface by Rabe *et al* [87, 88], providing indications of molecular structures and dynamics. In 2011, Zhong *et al* reported the polymerization of linear alkanes on Au(110) [89], where the C–H activation selectively took place at the sites of terminal $CH_3$ or penultimate $CH_2$ groups. In such a pioneering work, Au(110) surface served as both a platform and a catalyst for the alkyl C–H bond activation, and provided 1D constraint as well. A long-chain alkane, $C_{32}H_{66}$, was deposited and the sample was annealed to 440 K, leading to polymerization with formation of PE chains. The dehydrogenative polymerization process was further confirmed based on a control experiment of alkane chains with phenylene connections. High selectivity in the reaction sites of C($sp^3$)–H activation was thus determined by a combination of STM imaging and DFT calculations. This work opened the door of C–H activation on surfaces [90–94] and inspired on-surface activation of relatively inert functional groups typically like methyl and aryl groups. Recently, concentrating on the C($sp^3$)–H activation, Li *et al* discovered a novel phenomenon of direct transformation from *n*-alkane into *trans*-polyene [95] with the assistance of complementary microscopic and spectroscopic characterization techniques (figure 5(a)). By applying the same molecular precursor $C_{32}H_{66}$ yet different substrate, Cu(110), they showed the close-packed lamellar structure (left panel) upon molecular deposition at room temperature (RT). A low-flux and hot deposition strategy with a substrate temperature of 453 K, interestingly, led to the formation of monodispersed molecular chains as shown in the middle panel. The molecular topography and skeleton characterized by STM and nc-AFM displayed characteristic line features of in-plane C–H bonds (right panel). Furthermore, a cascade alkane-to-polyene dehydrogenation scenario was clarified based on experimental and theoretical investigations. Thereafter, the authors reported the coupling of polyenes on Cu(110) forming PA after thermal treatment at 470 K (figure 5(b)) [96]. Three types of connections were unambiguously distinguished from STM/nc-AFM images, including $\alpha$, $\beta$, and $\gamma$ types, which stemmed from different coupling ways of two terminal alkenyl groups. Among them, $\alpha$-type appeared in an all-*trans* configuration with a seamless morphology, while the other two were in *cis*

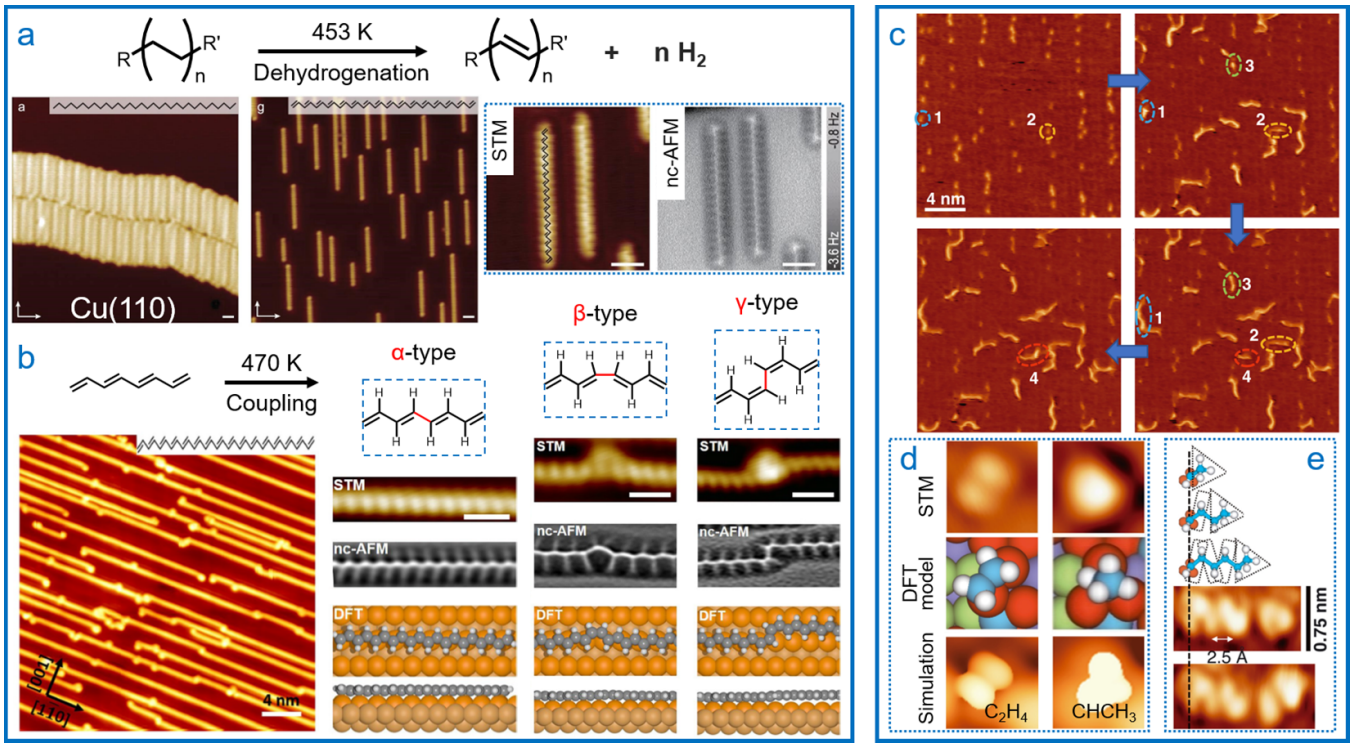


**Figure 5.** On-surface synthesis of polyacetylene, polyene, and polyethylene. (a) Dehydrogenation of *n*-alkanes to produce all-*trans* conjugated polyene on Cu(110). Reproduced from [95]. CC BY 4.0. (b) Coupling reaction of conjugated polyenes on Cu(110) with the formation of polyacetylene containing three different connections. Reproduced from [96], with permission from Springer Nature. (c) Polymerization of ethylene on a carburized iron single-crystal surface at RT. (d) An individual $C_2H_4$ molecule (left) and ethylidene ($CHCH_3$, right) captured by LT-STM imaging. (e) Polymer chain growth forming $C_8$ and $C_{10}$ chains. (c)–(e) From [97]. Reprinted with permission from AAAS.

configurations at the linkage with features of obvious protrusions. Note that the proportion of $\alpha$-type turned out to be related to the initial molecular coverage and could be effectively increased at a higher coverage. The series of studies presented the possibility of C–H activation of alkanes ($C(sp^3)$–H) as well as the transformation from alkanes to PAs (i.e. from $C(sp^3)$ to $C(sp^2)$), which would shed light on the exploitation of alkane feedstocks in an efficient and clean way.

PE, with a chemical formula of $(C_2H_4)_n$, is a mixture of polymers of ethylene (i.e. with various values of *n*) and widely used as plastics. The catalytic production of PE is of utmost importance in the chemical industry and attracts great interest from chemists. With such a motivation, Guo *et al* applied it as a model system and successfully visualized the activator-free polymerization process of ethylene forming PE on a carburized Fe(110) surface using STM [97]. They captured the *in-situ* chain growing process during continuous RT-STM scanning in a $C_2H_4$ atmosphere of $1 \times 10^{-8}$ mbar (figure 5(c)). Based on low temperature (LT) STM imaging, $C_2H_4$ (left) and $CHCH_3$ (right, as a chain initiator) were found in the initiation of polymer growth (figure 5(d)). Short PE chains (e.g. $C_8$ and $C_{10}$ chains) with triangularly shaped ends were revealed to grow by ethylene insertion (figure 5(e)), and a specific triangular Fe site at the domain boundary was the key for the polymerization. Such a real-space single-molecule-level investigation enriched the mechanistic understandings on the PE polymerization and should be significant for both chemistry and materials science.

In addition to the applications in the exploration of 1D PA and PE (involving $C(sp^2)$ and $C(sp^3)$, respectively), SPM techniques have also exhibited availability and versatility in the precise synthesis and fine characterization of 1D C(sp)-containing chain structures as well as interconversions between $sp^2$- and sp-hybridized carbon skeletons. The beginning of this century witnessed the precise control over initiation and termination of linear propagation of diacetylenes on graphite, which was stimulated by either an STM tip or UV light irradiation [98–100], forming extensive conjugated nanowires under ambient conditions. Recently, a series of organometallic or intrinsic polyynes have been fabricated on surfaces with atomic precision [23, 101–104] starting from various molecular precursors, as typically shown in figure 6. Based on the acetylene ($C_2H_2$) precursors, Xu *et al* have successfully synthesized *cis*-PAs, *trans*-PAs [105], and organometallic Cu-polyynes [101] (i.e. metalated carbynes, with a repeating unit of –C≡C–Cu–) on Cu(110) by applying different substrate temperatures (figure 6(a)). Upon deposition of $C_2H_2$ at 300 K and mild annealing, a mixture of *cis*- and *trans*-PA segments formed, and a *cis*-to-*trans* isomerization could be triggered by further thermal treatment. High-resolution STM and nc-AFM images provided both morphology and skeleton information, and accordingly, determined the corresponding

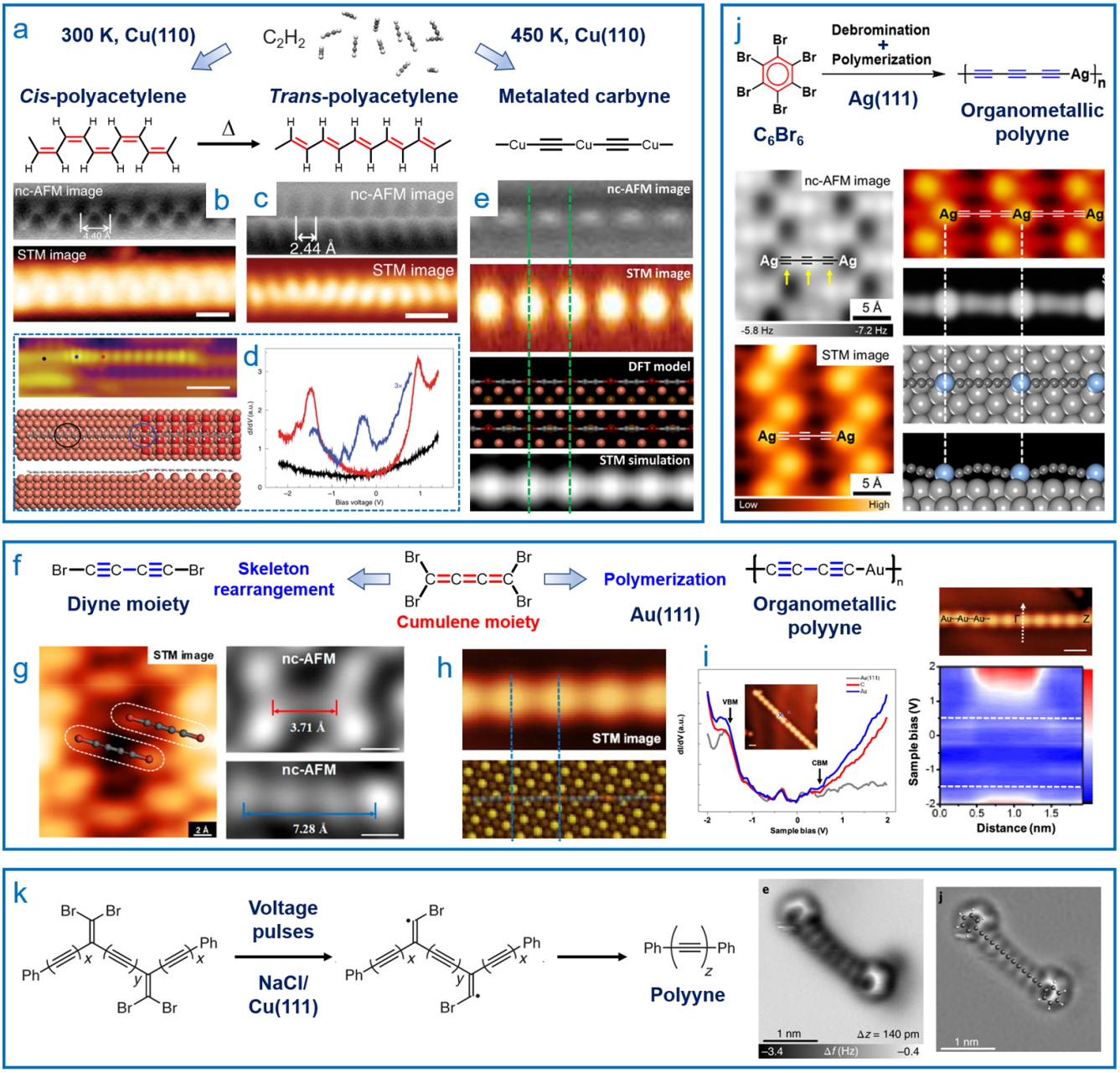


**Figure 6.** On-surface synthesis and characterization of a series of polyacetylenes, organometallic and intrinsic polyynes. (a)–(e) Synthesis and characterization of *cis*- and *trans*-polyacetylenes and Cu-carbyne on Cu(110) by applying $C_2H_2$ as precursor. (b)–(d) Reproduced from [105], with permission from Springer Nature. (e) Reprinted with permission from [101]. Copyright (2016) American Chemical Society. (f)–(i) Synthesis and characterization of 1D diacetylenic Au-carbyne on Au(111). (g)–(i) Reprinted with permission from [102]. Copyright (2020) American Chemical Society. (j) Triacetylenic Ag-carbyne on Ag(111). Reprinted with permission from [103]. Copyright (2022) American Chemical Society. (k) *In-situ* synthesis of polyynes on NaCl/Cu(111). Reproduced from [23], with permission from Springer Nature.

structures (figures 6(b) and (c)). Interestingly, by constructing oxides on the substrate, the hybridization between *trans*-PA chains and underlying layer was highly reduced compared to that in the case of bare surface. An interface state (middle, indicated in blue) was discovered between the metal- (left, indicated in black) and oxide-supported *trans*-PA segments (right, indicated in red) from both STM image and d$I$/d$V$ spectra (figure 6(d)), revealing the metallic-to-semiconducting transformation. Moreover, metalated carbynes were synthesized after deposition of $C_2H_2$ onto Cu(110) held at 450 K. Notably, the C–C triple bonds appeared as bright features in the nc-AFM image, while the incorporated Cu atoms were only visible in the STM image as bright protrusions (figure 6(e)). Apart from the strategy of C(sp)–H activation, Yu *et al* further applied C(sp$^2$)–$Br_2$ activation based on cumulene moiety and synthesized the 1D diacetylenic Au-carbyne (–$C_4$–Au–)

as another organometallic polyyne on Au(111) (figure 6(f)) [102]. By applying a voltage pulse locally on the molecular precursors at LT, they observed the cleavage of two C–Br bonds and a simultaneous topographic transformation from a shape of dog bone to a linear one (figure 6(g)). A combination of STM and nc-AFM imaging further corroborated the skeleton rearrangement from a cumulene moiety to a diyne one (Br–C≡C–C≡C–Br). In contrast, deposition of precursors at RT directly led to the fabrication of Au-carbyne (figure 6(h)). The band gap was experimentally determined to be ∼2.0 eV on Au(111) by STS, indicating a semiconducting feature (figure 6(i)). Recently, the family of organometallic polyynes was further extended to triacetylenic Ag-carbyne by the same group [103]. Starting from $C_6Br_6$ molecules, an unexpected ring-opening process of $C_6$ rings was triggered along with a complete debromination on Ag(111) at 300 K, leading to the formation of Ag-carbyne chains with a repeating unit of –$(C{\equiv}C)_3$–Ag– (figure 6(j)). The characteristic features were clearly shown in the STM/nc-AFM images and nicely reproduced by DFT calculations. Furthermore, the transformation between metallic carbynes with different periodicities was investigated, from –C≡C–Ag– to –$(C{\equiv}C)_2$–Ag– on Ag(110) and from –$(C{\equiv}C)_2$–Cu– to –C≡C–Cu– on Cu(110) [104]. Such a skeleton reconstruction was revealed to originate from the corresponding thermodynamic stability by extensive DFT calculations. It was also theoretically predicted that the band gap of organometallic polyynes would be highly related to the number of C–C triple bonds involved (acetylenic > diacetylenic > triacetylenic Ag/Cu/Au-carbyne) as well as the incorporated metal elements (Ag-carbyne > Cu-carbyne > Au-carbyne).

Moreover, intrinsic polyyne, with consecutive sp-carbon atoms, is promising for applications as molecular wires for charge transport in electronic circuitry [106]. Due to the instability and high reactivity of multiple alkynyl groups (–C≡C–) involved in polyene (which is also the case of 0D cyclocarbon), the synthesis of intrinsic polyyne has long been a challenging topic. By functionalization of bulky terminal groups as end-caps to stabilize the long –$(C{\equiv}C)_n$– chain structures, the electrical conductance of oligoynes ($n$ = 1, 2, 4) has been directly detected by STM-molecular break junction techniques [106]. Significantly, by virtue of atomic manipulation (that is, applying voltage pulses on the target position of molecular precursors), Pavliček *et al* fabricated a long polyyne, Ph–$(C{\equiv}C)_8$–Ph, on NaCl/Cu(111) via skeleton rearrangement and monitored the whole process by nc-AFM and STM (figure 6(k)) [23]. They applied a molecule containing 1,1-dibromo alkenes as precursor and precisely cleaved the C–Br bonds *in situ* by a qPlus-based STM/AFM tip, which was followed by the rearrangement of remaining carbon skeleton, forming various polyenes ($n$ = 3, 4, 6, 8). STS indicated that the LUMO energies of polyyne family decreased as the value of n increased, resulting in a reduced band gap (in good agreement with that in the case of organometallic polyynes as discussed above). This study thus demonstrates the versatility of SPM techniques in the aspects, including but not limited to bond-resolved topographic and skeletal characterization [70, 107–110], orbital imaging [111–114], triggering reactions *in situ* [115–117], visualization of reaction pathways [22, 32, 117], and detection of properties [70, 81, 118–121] (e.g. electronic and magnetic).

The applications of SPM in the 1D nanostructures and nanomaterials typically like PE, PA, and (organometallic) polyyne thus unraveled an interesting interplay among $C(sp^3)$, $C(sp^2)$, and C(sp), as well as the interconversions among alkyl, alkenyl, and alkynyl groups and the corresponding halo-substituted functional groups. The methodologies and on-surface synthesis strategies open a new window on novel carbon-based materials, especially on the atomically precise fabrication of highly reactive and unstable carbon-based chains, which would otherwise be hindered in conventional solution chemistry due to obstacles such as cross-linking, cycloaddition, solubility, isolation, and purification.

### 3.2. GNRs and other π-conjugated polymer chains

Graphene is known as a 2D single-atom-thin carbon layer [4] embedded with $C(sp^2)$ hexagonal rings, which is a semimetal with a zero band gap. When it is laterally confined to the nanometer scale, for instance, 1D ribbons, the band gap opens. GNRs thus emerge as a promising 1D carbon nanostructure as well as an attractive research topic due to their outstanding electronic properties. As the band gap is crucially dependent on the topologies of GNRs (such as width of ribbons [122] and their edge geometries [123]), preparation of GNRs with atomic precision is a prerequisite. Since the pioneering bottom-up fabrication of armchair GNR (7-AGNR) reported by Cai *et al* in 2010 [124], on-surface synthesis strategy has displayed its capability in the subtle regulation of the topologies and consequently precise steering of the electronic properties. So far, GNRs with AGNRs and zigzag edges [124–126], chiral GNRs [121, 127, 128], heteroatom-doped GNRs [120, 129–131], and extended nanoporous graphenes [132, 133] have been precisely synthesized on surfaces and extensively investigated by virtue of SPM techniques. Several strategies turn out to be effective in tuning the band gaps. A common method is increasing the width by the rational selection of molecular precursors, for example, 13-AGNRs and 9-AGNRs have a similar band gap of ∼1.4 eV on Au(111) [134, 135] while ∼2.3–2.5 eV for 7-AGNRs as experimentally determined by STS [134, 136]. Moreover, topological band engineering by forming heterojunctions [137, 138], for instance, by the integration of alternating topologically trivial 7-AGNR and topologically nontrivial 9-AGNR components [137, 139, 140] forming 7/9-AGNR heterojunctions, was also reported, which resulted in the formation of interface states within 1D ribbons and new bulk frontier bands. Profiting from this remarkable effort, semi-conducting GNRs have been prepared with the band gaps reduced to ∼0.74 eV for the 7/9-AGNR [137] and ∼0.65 eV for the 7-AGNR-S(1,3) [138].

Interestingly, Rizzo *et al* reported the formation of metallic GNRs for the first time by introducing a symmetric superlattice of zero-energy modes into GNRs [118] as shown in figure 7. Starting from the delicately designed molecular precursor 1 with dibromo-substitution and a methyl group,

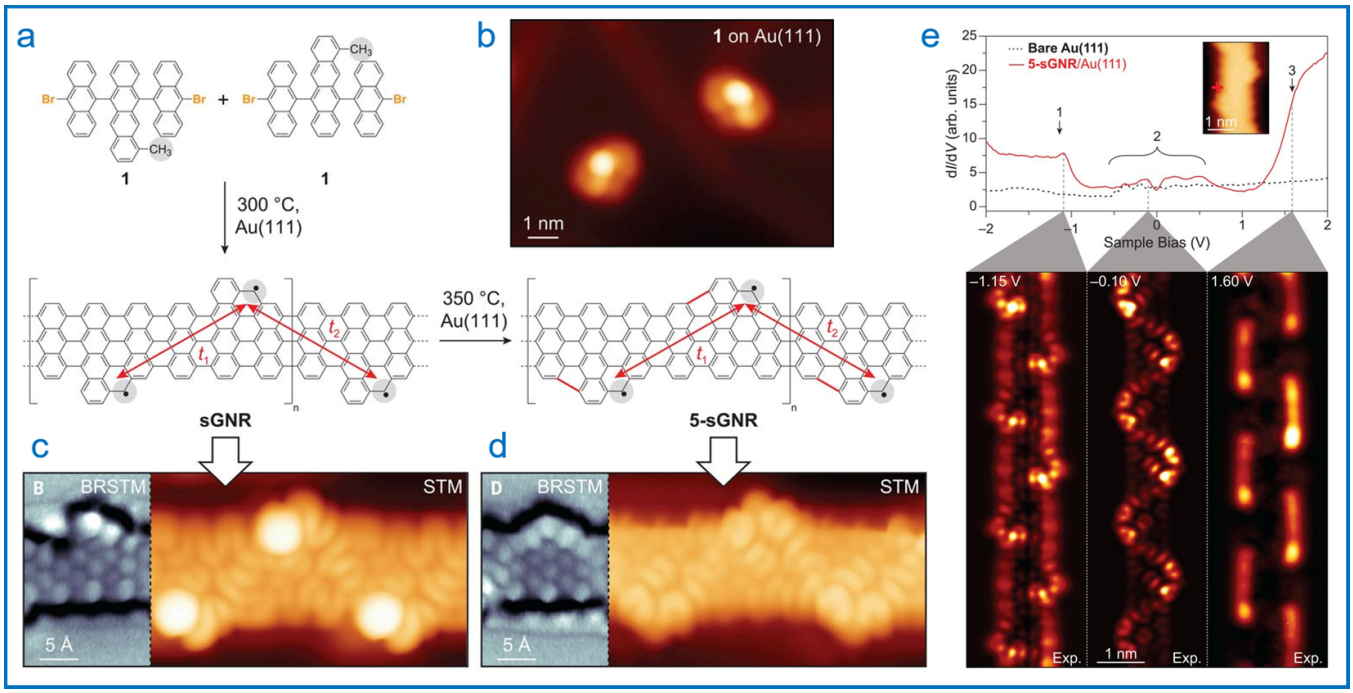


**Figure 7.** On-surface synthesis and characterization of graphene nanoribbons including sGNR and 5-sGNR. (a) Synthesis of 5-sGNR on Au(111) from molecular precursor 1 with the formation of sGNR as an intermediate state. (b)-(d) STM images of (b) molecular precursor 1, (c) an isolated sGNR, and (d) 5-sGNR on Au(111). (e) d*I*/d*V* spectra and mapping of 5-sGNR on Au(111). State 1, state 3, and state 2 showed the valence band, conduction band, and zero-mode band, respectively. From [118]. Reprinted with permission from AAAS.

they followed the routine recipe of Ullmann coupling and cyclodehydrogenation and synthesized sawtooth-GNRs (sGNRs) on Au(111) at 300 °C (figures 7(a) and (b)). Surprisingly, further annealing at 300 °C resulted in the transformation to the 5-sGNRs with the fusion of five-membered rings along the cove edges. The superposition of two H atoms at the cove regions of sGNRs caused the nonplanar configuration and thus appeared as periodic bright dots at both edges in the STM image (figure 7(c)), which disappeared in the 5-sGNRs with a planar configuration (figure 7(d)). BRSTM imaging by mapping the d*I*/d*V* signal at a low bias further unambiguously proved the structures involved (figures 7(c) and (d)). The sGNR was revealed to have a sharp peak near Fermi level showing a metallic feature on Au(111) by d*I*/d*V* spectra, which was theoretically calculated to be induced by the underlying substrate. Nevertheless, the construction of pentagonal rings brought about a robust metallicity with a wider bandwidth, shown as a broad density of states feature that spans Fermi level (state 2) in the d*I*/d*V* spectra (upper panel of figure 7(e)), which was further calculated to be independent of the substrate. The d*I*/d*V* maps displayed the local density of states (LDOS) at the edges of valence band, zero-mode band, and conduction band, respectively (cf lower panel of figure 7(e)). The modification of zero-mode superlattices accompanied by the STM/STS evidences revealed a feasible methodology to induce and explore the metallicity in not only GNRs but also other carbon-based nanostructures. More relevant studies in the regard of on-surface synthesis of GNRs and their outstanding electronic properties have been nicely reviewed by Talirz *et al* [123], and the correlation between topological structures and electronic states of graphene could be found in the review paper by Li *et al* [141]. In addition, some GNR-like ribbons with nonhexagonal carbon rings [142–146] have also been exploited with the purpose of fine tuning of their electronic properties.

Additionally, numerous 1D $\pi$-conjugated polymers have been explored as an extension from GNRs and GNR-like nanostructures. One promising way is the incorporation of *n*-membered rings with $\pi$ conjugation based on C($sp^2$), for example, preparation of 1D $\pi$-conjugated polymers with indenofluorene units where five-membered rings were incorporated [147]. Alternatively, C(sp)-containing skeletons have been successfully embedded in the $sp^2$-hybridized GNRs and GNR-like nanostructures for better electronic tailoring, such as ethynylene-bridged [148–151], diacetylene-bridged [152, 153], and cumulene-bridged [154, 155] polymers. Besides, 1D cumulene-linked polymers with the involvement of five- and seven-membered rings (based on a tribenzoazulene building block) [156] was also achieved. Notably, Cirera *et al* explored the topological order involved in such $\pi$-conjugated polymers [157] as shown in figure 8. 1D C(sp)-bridged acene-containing polymers were synthesized on Au(111) using the same strategy (figure 8(a)), which was based on precursors with various acene units (including anthracene, pentacene, and bisanthene). The nc-AFM characterization (figure 8(b)) provided clear features of bisanthene units and linear bridges, which were attributed to cumulene (=C=C=) links instead of ethynylene (–C≡C–) ones. It is

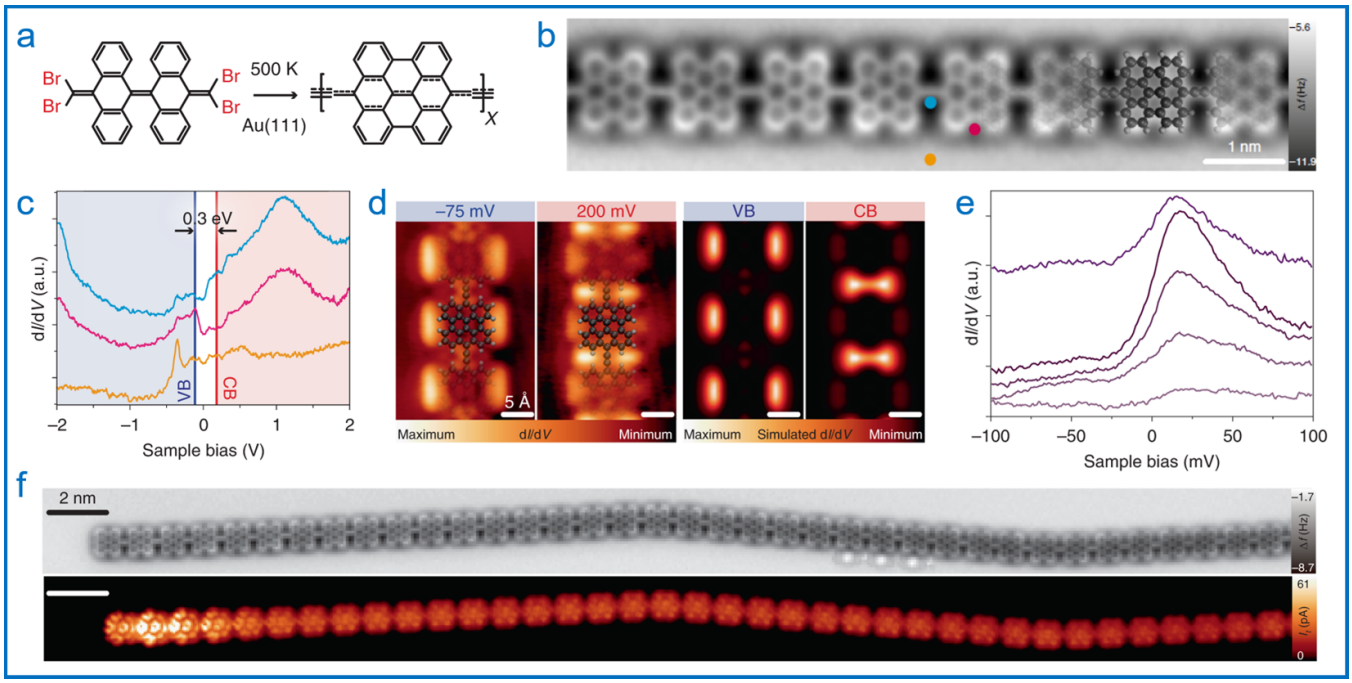


**Figure 8.** On-surface synthesis and characterization of 1D $\pi$-conjugated polymers. (a) Synthesis of $\pi$-conjugated polymers comprising bisanthene units. (b) Nc-AFM image resolving the chain skeletons. (c) d$I$/d$V$ spectra conducted at the corresponding positions marked in (b). (d) d$I$/d$V$ mapping and simulations obtained at the edges of valence band and conduction band. (e) d$I$/d$V$ spectra showing the distribution of the edge state. The sequence from top to bottom corresponds to the sites from the termination of the polymer to the center. (f) Nc-AFM and STM images of the $\pi$-conjugated polymer. Reproduced from [157], with permission from Springer Nature.

worth noting that the topological phase transition between ethynylene-linked acene and cumulene-linked quinoid structure strongly depends on the size of acene unit involved. Owing to the formation of quinoid-cumulene resonant form, a narrow band gap of ∼0.3 eV was detected from the d$I$/d$V$ spectra (figure 8(c)). The LDOS at the edges of valence band (∼−75 meV) and conduction band (∼200 meV) was visualized by d$I$/d$V$ mapping (figure 8(d)), showing an obvious electronic swap compared to the case involving anthracene units. Furthermore, the in-gap zero-energy edge state was directly observed to fade away from the termination to the center in the d$I$/d$V$ spectra (figure 8(e), from top to bottom) and STM image (figure 8(f)). Such a study revealed the interplay between resonant forms and topological quantum phases, and successfully engineered the 1D $\pi$-conjugated polymers to have narrow band gaps and zero-energy edge states, which would be inspirational for fabricating intrinsic metallic polymers.

## 4. 2D carbon-based nanostructures and nanomaterials

By further extending the lateral width from 1D GNRs, GNR-like ribbons, and other $\pi$-conjugated polymer chains, some 2D novel carbon-based nanostructures have been obtained, such as extended nanoporous graphenes [132, 133] as mentioned above. Among them, one recent exciting example is the synthesis of biphenylene network [119], a nonbenzenoid carbon allotrope composed of 4–6–8 membered rings of C($sp^2$), which was achieved by on-surface interpolymer hydrogen-fluorine-zipping reaction on Au(111). The utilization of SPM techniques provided real-space characterization of the detailed structure and metallicity, indicating that it would be up-and-coming for conductive applications in carbon-based circuitry. Despite these achievements, it is actually quite challenging to perfectly extend the dimension of nanostructures from 1D to 2D with controlled covalent bonding based on on-surface synthesis. One of the difficulties lies in the synthetic strategy, which is dominated by a routine recipe of Ullmann-type-based (C–X) coupling independently [158] or followed by cyclodehydrogenation [132], generally resulting in the poor selectivity in the multiple reaction sites, generation of metal-incorporated reaction intermediates, appearance of excessive halogen byproducts in the vicinity, etc. These unavoidable factors or phenomena prohibit researchers from processing toward 2D large-scale and uniform carbon-based nanostructures and nanomaterials with designed structures and patterns. To overcome these aspects, high-dilution strategy [159] on hot substrates would be a good option. In addition, developing novel on-surface reaction types with higher selectivity and less byproducts is in desperate need. In this regard, H–F zipping [119, 160] as mentioned above shows high efficiency. More recently, a programable hierarchical synthetic strategy was reported by Tenorio *et al* based on a subtle combination of Ullmann coupling, cyclodehydrogenation, and H–Cl zipping [133], leading to the fabrication of 2D hybrid nanoporous graphene. Interestingly, GNRs prepared

in the first step (using the first component) was designed to serve as a dynamic template providing nanochannels for fusing with the second component, and consequently, the 1D GNRs laterally extended to 2D. Nevertheless, further efforts in developing synthetic strategy and preparing 2D carbon-based nanostructures with atomic precision would be prerequisite for fine characterization and precise measurement. Leaving aside these challenges in synthesis, carbon-based nanostructures and nanomaterials characterized by SPM share similarity in features at different dimensions, and the related studies will not be focused herein.

In addition to the UHV-SPM combined with on-surface synthesis strategy as mainly discussed above, which highly relies on the catalytic property and 2D confinement of the underlying metal substrates, the application of SPM under ambient conditions or in direct connection with solution chemistry has also shown its great contribution in understanding carbon-based nanostructures and nanomaterials and the corresponding chemical processes. In ambient conditions, highly oriented pyrolytic graphite (HOPG), which has weak hybridization with adsorbed structures and is generally inert, provides an alternative platform for such investigations, untangling the intrinsic chemical activities. For example, nucleation-elongation processes are approachable and could be directly monitored on HOPG at the molecular scale under ambient conditions [161] based on SPM. As reported by Zhan *et al* recently, STM revealed time-dependent evolution of the dynamic polymerization and crystallization processes at the solid-liquid interface in real space [161], which provided mechanistic and kinetic insights into the construction of 2D covalent polymers. Besides, highly ordered 2D covalent organic frameworks (COFs) could be directly fabricated using various strategies and explored at interfaces [162], such as aldehyde-amine condensation via a solid-vapor interface reaction [163] and a self-condensation of diboronic acid at the liquid-solid interface [164]. More features about these graphene-like single-layered COF structures and their STM studies could be found in the review paper [165]. Moreover, *in-situ* observation and detection offered by SPM under ambient conditions provides possibilities to bridge the pressure gap between UHV-based experiments and real world for the exploitation of carbon-based nanomaterials.

## 5. Summary and outlook

STM and AFM become more and more indispensable and extremely versatile in the atomic-scale exploration of low-dimensional carbon-based nanostructures and nanomaterials. Dependent on the UHV conditions, UHV-SPM has shown its great contribution to a series of sophisticated procedures on surfaces in combination with on-surface synthesis strategy, including induction of localized chemical reactions with simultaneous monitoring, determination of unknown structures with unambiguous skeletal characterization, visualization of reaction pathways with detection of intermediate states, identification of electronic and magnetic configurations, revelation of structure-activity relationship, etc. In this review, we mainly discussed the applications of STM and AFM in probing several typical carbon-based nanostructures and nanomaterials at different dimensions concerning the above aspects, ranging from novel carbon allotropes to hydrocarbons and carbon-based organometallic structures. Besides, intriguing interconversions among $C(sp^3)$, $C(sp^2)$, and C(sp) were also displayed and corroborated in real space, indicating the regulation rules of $sp^n$-hybridized carbons involved in the corresponding nanostructures and nanomaterials. Therefore, STM/AFM opens up new frontiers in chemical synthesis, structural characterization, and property measurement with atomic precision.

Nevertheless, some improvements are expected to promote broader application of these techniques as concisely illustrated in figure 9. The first point would be visualizing the chemical arrangement of carbon-based nanostructures (including both chemical element and spatial arrangement), in other words, the combination of chemical sensitivity and skeletal information. Although the current advance in STM/AFM has made it possible to discriminate different bond orders as well as skeletons (spatial arrangements) involved in the relatively planar structures as extensively displayed above, STM/AFM is still suffering from the lack of chemical sensitivity that requires characteristic fingerprints related to specific chemical bonds or groups. The combination of complementary spectroscopic information and topographic one provided by STM/AFM has shown its feasibility in this aspect (cf upper left panel of figure 9). For instance, application of tip-enhanced Raman spectroscopy (TERS) [166, 167] and STM/AFM has been demonstrated to be capable of determining structural and chemical heterogeneities in the dehydrogenation processes at the single-bond limit [168] and identifying $\pi$-skeletons in coupling reactions [155], where the characteristic vibrational motions originated from specific bonds are the key to such chemical sensitivity. Moreover, TERS measurements have been shown to provide chemical information both laterally and vertically [167, 168], which offer access to nonplanar stereo structures [167] and even more general 3D nanostructures. Meanwhile, it is also highly desirable to develop imaging techniques or methodologies of STM/AFM itself to characterize general 3D molecular skeletons.

In addition, on-surface synthesis of carbon-based nanostructures and nanomaterials strongly relies on either thermal excitation or atom manipulation (by means of injecting tunneling electrons) so far, while other extensive excitation sources (such as photo-excitation [169–173] and localized surface plasmons [174–177] as illustrated in the bottom panel of figure 9) have been much less reported or applied in synthesis. Given that thermal excitation would activate several chemical groups simultaneously, poor reaction selectivity has long been a realistic obstacle. Besides, for pericyclic reactions, selection rules (also known as Woodward Hoffmann rules) indicate that some reactions would be ground state (thermally) allowed, while others would be excited state (photochemically) allowed yet thermally forbidden. Notably, plasmon-induced reactions by confining light at the SPM junction can significantly reduce the energy requirements and facilitate efficient energy conversion with a strong enhancement of the electric field [174, 176, 177]. Thus, integration of a broader range

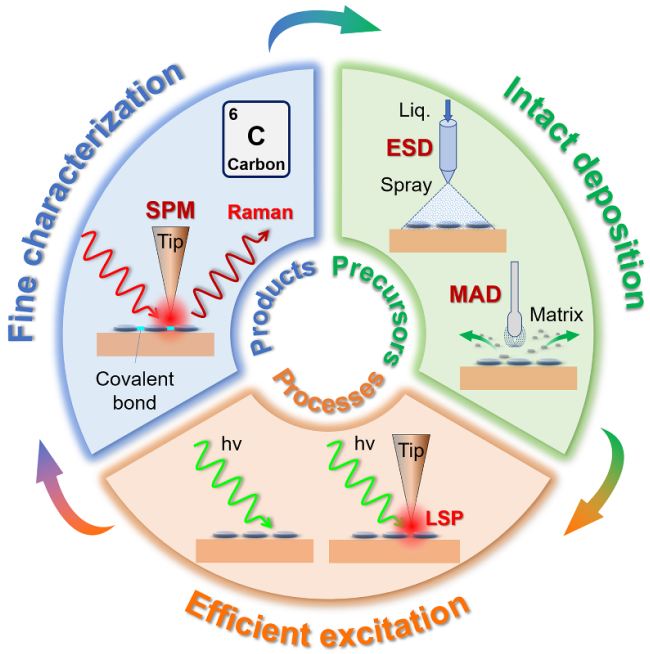


**Figure 9.** Schematic illustration of the prospect of SPM techniques in probing low-dimensional carbon-based nanostructures and nanomaterials.

of excitation sources into on-surface synthesis and STM/AFM technique should provide complementary and alternative solutions for fabrication and exploration of novel carbon-based nanostructures and nanomaterials.

Moreover, intact deposition of carbon-based molecular precursors or structures is not only prerequisite for on-surface synthesis protocol, but also essential for direct investigation under UHV conditions (cf upper right panel of figure 9). Traditional thermal sublimation is generally available for relatively small organic molecules, while it may not be applicable to those with larger molecular mass due to side reactions before or during evaporation (that is, fragility of structures), for example, the macrocycle 1 shown in figure 4(d). In this regard, methods typically like flash-annealing a silicon wafer loaded with large compounds [79] and electrospray deposition (ESD) under UHV conditions (UHV-ESD) [178–180] have been demonstrated to be effective and powerful. Nonetheless, a high ratio of polymeric fragments could still be found (e.g. ∼92% [79] in the study of figure 4(d)) coexisting with intact ones in the former case, while a mixture of solvent and solute would be present on surfaces based on UHV-ESD method [179, 180]. Recently, a hybrid bottom-up approach toward GNRs called matrix-assisted direct transfer technique [181] by a win-win combination of solution-based polymerization and on-surface synthesis was reported. Carbon-based polymer sample dispersed in an inert matrix was loaded into a fiberglass applicator under ambient conditions and was further transferred onto a substrate in UHV. Thereafter, the bulk matrix was easily removed from surface by annealing, followed by on-surface cyclodehydrogenation reactions of polymers forming GNRs. Such a technique would be promising not only in directly bridging the gaps between solution chemistry and UHV conditions, but also in the synergy between both bottom-up approaches (i.e. solution-based and on-surface synthesis). It is also eagerly expected to develop similar techniques or expand the database of polymer-matrix association to further extend this concept to the synthesis and exploration of more general carbon-based nanostructures and nanomaterials, which would greatly suppress the limitations of either synthetic method and bring the superiority of SPM into full play.

Furthermore, despite the significant role played by STM and AFM, several variations of STM and AFM have emerged and expanded the family of SPM, for example, pump-probe STM with time resolution [182–184], spin-polarized STM [185–187], near-field SPM (typically like TERS as mentioned above) [166, 188–192], Kelvin probe force microscopy [193, 194], etc. These variations of SPM are expected to provide more and more influence over the carbon-based electronics and spintronics.

The understanding of carbon-based nanostructures and nanomaterials will be further enriched by comprehensive consideration on the above several aspects, which will also open an avenue for the exploration and development of elusive and undiscovered carbon-based nanomaterials.

## Acknowledgments

The authors acknowledge financial support from the National Natural Science Foundation of China (Grant Nos. 22125203, 21790351), and the Fundamental Research Funds for the Central Universities (Grant No. 22120220051).

## Conflict of interest

The authors declare that they have no conflict of interest.

## ORCID iD

Wei Xu https://orcid.org/0000-0003-0216-794X

## References

[1] Hirsch A 2010 The era of carbon allotropes *Nat. Mater.* **9** 868–71
[2] Kroto H W, Heath J R, O'Brien S C, Curl R F and Smalley R E 1985 $C_{60}$: buckminsterfullerene *Nature* **318** 162–3
[3] Iijima S 1991 Helical microtubules of graphitic carbon *Nature* **354** 56–58
[4] Novoselov K S, Geim A K, Morozov S V, Jiang D, Zhang Y, Dubonos S V, Grigorieva I V and Firsov A A 2004 Electric field effect in atomically thin carbon films *Science* **306** 666–9
[5] Bottari G and Torres T 2017 A new dimension for low-dimensional carbon nanostructures *Chem* **3** 21–24
[6] Li G, Li Y, Liu H, Guo Y, Li Y and Zhu D 2010 Architecture of graphdiyne nanoscale films *Chem. Commun.* **46** 3256–8
[7] Li Y, Xu L, Liu H and Li Y 2014 Graphdiyne and graphyne: from theoretical predictions to practical construction *Chem. Soc. Rev.* **43** 2572–86

[8] Gao X, Liu H, Wang D and Zhang J 2019 Graphdiyne: synthesis, properties, and applications *Chem. Soc. Rev.* **48** 908–36

[9] Chalifoux W A and Tykwinski R R 2010 Synthesis of polyynes to model the sp-carbon allotrope carbyne *Nat. Chem.* **2** 967–71

[10] Liu M, Artyukhov V I, Lee H, Xu F and Yakobson B I 2013 Carbyne from first principles: chain of C atoms, a nanorod or a nanorope *ACS Nano* **7** 10075–82

[11] Tongay S, Senger R T, Dag S and Ciraci S 2004 *Ab-initio* electron transport calculations of carbon based string structures *Phys. Rev. Lett.* **93** 136404

[12] Li X, Zhang H and Chi L 2018 On-surface synthesis of graphyne-based nanostructures *Adv. Mater.* **31** 1804087

[13] Chen H, Zhu H, Huang Z, Rong W and Wu K 2019 Two-sidedness of surface reaction mediation *Adv. Mater.* **31** 1902080

[14] Shen Q, Gao H-Y and Fuchs H 2017 Frontiers of on-surface synthesis: from principles to applications *Nano Today* **13** 77–96

[15] Grill L and Hecht S 2020 Covalent on-surface polymerization *Nat. Chem.* **12** 115–30

[16] Dong L, Liu P N and Lin N 2015 Surface-activated coupling reactions confined on a surface *Acc. Chem. Res.* **48** 2765–74

[17] Klappenberger F, Zhang Y-Q, Björk J, Klyatskaya S, Ruben M and Barth J V 2015 On-surface synthesis of carbon-based scaffolds and nanomaterials using terminal alkynes *Acc. Chem. Res.* **48** 2140–50

[18] Held P A, Fuchs H and Studer A 2017 Covalent-bond formation via on-surface chemistry *Chem. Eur. J.* **23** 5874–92

[19] Clair S and de Oteyza D G 2019 Controlling a chemical coupling reaction on a surface: tools and strategies for on-surface synthesis *Chem. Rev.* **119** 4717–76

[20] Bian K, Gerber C, Heinrich A J, Müller D J, Scheuring S and Jiang Y 2021 Scanning probe microscopy *Nat. Rev. Methods Primers* **1** 36

[21] Gross L, Schuler B, Pavliček N, Fatayer S, Majzik Z, Moll N, Peña D and Meyer G 2018 Atomic force microscopy for molecular structure elucidation *Angew. Chem., Int. Ed.* **57** 3888–908

[22] Kaiser K, Scriven L M, Schulz F, Gawel P, Gross L and Anderson H L 2019 An sp-hybridized molecular carbon allotrope, cyclo[18]carbon *Science* **365** 1299–301

[23] Pavliček N, Gawel P, Kohn D R, Majzik Z, Xiong Y, Meyer G, Anderson H L and Gross L 2018 Polyyne formation via skeletal rearrangement induced by atomic manipulation *Nat. Chem.* **10** 853–8

[24] Otero G *et al* 2008 Fullerenes from aromatic precursors by surface-catalysed cyclodehydrogenation *Nature* **454** 865–8

[25] Amsharov K, Abdurakhmanova N, Stepanow S, Rauschenbach S, Jansen M and Kern K 2010 Towards the isomer-specific synthesis of higher fullerenes and buckybowls by the surface-catalyzed cyclodehydrogenation of aromatic precursors *Angew. Chem., Int. Ed.* **49** 9392–6

[26] Pinardi A L *et al* 2013 Tailored formation of N-doped nanoarchitectures by diffusion-controlled on-surface (cyclo)-dehydrogenation of heteroaromatics *ACS Nano* **7** 3676–84

[27] Pinardi A L, Martínez J I, Jančařík A, Stará I G, Starý I, López M F, Méndez J and Martín-Gago J Á 2014 Sequential formation of N-doped nanohelicenes, nanographenes and nanodomes by surface-assisted chemical (cyclo)dehydrogenation of heteroaromatics *Chem. Commun.* **50** 1555–7

[28] Lu J, Yeo P S E, Gan C K, Wu P and Loh K P 2011 Transforming $C_{60}$ molecules into graphene quantum dots *Nat. Nanotechnol.* **6** 247–52

[29] Gross L, Mohn F, Moll N, Liljeroth P and Meyer G 2009 The chemical structure of a molecule resolved by atomic force microscopy *Science* **325** 1110–4

[30] Giessibl F J 2019 The qPlus sensor, a powerful core for the atomic force microscope *Rev. Sci. Instrum.* **90** 11101

[31] Gross L, Mohn F, Moll N, Schuler B, Criado A, Guitián E, Peña D, Gourdon A and Meyer G 2012 Bond-order discrimination by atomic force microscopy *Science* **337** 1326–9

[32] Moreno C, Stetsovych O, Shimizu T K and Custance O 2015 Imaging three-dimensional surface objects with submolecular resolution by atomic force microscopy *Nano Lett.* **15** 2257–62

[33] Scriven L M, Kaiser K, Schulz F, Sterling A J, Woltering S L, Gawel P, Christensen K E, Anderson H L and Gross L 2020 Synthesis of cyclo[18]carbon via debromination of $C_{18}Br_6$ *J. Am. Chem. Soc.* **142** 12921–4

[34] Müllen K and Rabe J P 2008 Nanographenes as active components of single-molecule electronics and how a scanning tunneling microscope puts them to work *Acc. Chem. Res.* **41** 511–20

[35] Fujii S and Enoki T 2013 Nanographene and graphene edges: electronic structure and nanofabrication *Acc. Chem. Res.* **46** 2202–10

[36] Son Y-W, Cohen M L and Louie S G 2006 Energy gaps in graphene nanoribbons *Phys. Rev. Lett.* **97** 216803

[37] Zuzak R *et al* 2018 Building a 22-ring nanographene by combining in-solution and on-surface syntheses *Chem. Commun.* **54** 10256–9

[38] Mishra S, Beyer D, Berger R, Liu J, Gröning O, Urgel J I, Müllen K, Ruffieux P, Feng X and Fasel R 2020 Topological defect-induced magnetism in a nanographene *J. Am. Chem. Soc.* **142** 1147–52

[39] Rogers C, Chen C, Pedramrazi Z, Omrani A A, Tsai H-Z, Jung H S, Lin S, Crommie M F and Fischer F R 2015 Closing the nanographene gap: surface-assisted synthesis of peripentacene from 6,6′-bipentacene precursors *Angew. Chem., Int. Ed.* **54** 15143–6

[40] Wang X-Y *et al* 2017 Heteroatom-doped perihexacene from a double helicene precursor: on-surface synthesis and properties *J. Am. Chem. Soc.* **139** 4671–4

[41] Telychko M *et al* 2021 Ultrahigh-yield on-surface synthesis and assembly of circumcoronene into a chiral electronic Kagome-honeycomb lattice *Sci. Adv.* **7** eabf0269

[42] Zhong Q *et al* 2019 Benzo-fused periacenes or double helicenes? Different cyclodehydrogenation pathways on surface and in solution *J. Am. Chem. Soc.* **141** 7399–406

[43] Hu Y, Wang X-Y, Peng P-X, Wang X-C, Cao X-Y, Feng X, Müllen K and Narita A 2017 Benzo-fused double [7]carbohelicene: synthesis, structures, and physicochemical properties *Angew. Chem., Int. Ed.* **56** 3374–8

[44] Mishra S, Lohr T G, Pignedoli C A, Liu J, Berger R, Urgel J I, Müllen K, Feng X, Ruffieux P and Fasel R 2018 Tailoring bond topologies in open-shell graphene nanostructures *ACS Nano* **12** 11917–27

[45] Mishra S *et al* 2020 Topological frustration induces unconventional magnetism in a nanographene *Nat. Nanotechnol.* **15** 22–28

[46] Mishra S *et al* 2021 Large magnetic exchange coupling in rhombus-shaped nanographenes with zigzag periphery *Nat. Chem.* **13** 581–6

[47] Buttrick J C and King B T 2017 Kekulenes, cycloarenes, and heterocycloarenes: addressing electronic structure and aromaticity through experiments and calculations *Chem. Soc. Rev.* **46** 7–20

[48] Pozo I, Majzik Z, Pavliček N, Melle-Franco M, Guitián E, Peña D, Gross L and Pérez D 2019 Revisiting kekulene: synthesis and single-molecule imaging *J. Am. Chem. Soc.* **141** 15488–93

[49] Treier M, Pignedoli C A, Laino T, Rieger R, Müllen K, Passerone D and Fasel R 2011 Surface-assisted cyclodehydrogenation provides a synthetic route towards easily processable and chemically tailored nanographenes *Nat. Chem.* **3** 61–67

[50] Su J, Wu X, Song S, Telychko M and Lu J 2020 Substrate induced strain for on-surface transformation and synthesis *Nanoscale* **12** 7500–8

[51] Shiotari A, Nakae T, Iwata K, Mori S, Okujima T, Uno H, Sakaguchi H and Sugimoto Y 2017 Strain-induced skeletal rearrangement of a polycyclic aromatic hydrocarbon on a copper surface *Nat. Commun.* **8** 16089

[52] Fan Q, Martin-Jimenez D, Werner S, Ebeling D, Koehler T, Vollgraff T, Sundermeyer J, Hieringer W, Schirmeisen A and Gottfried J M 2020 On-surface synthesis and characterization of a cycloarene: $C_{108}$ graphene ring *J. Am. Chem. Soc.* **142** 894–9

[53] Di Giovannantonio M, Yao X, Eimre K, Urgel J I, Ruffieux P, Pignedoli C A, Müllen K, Fasel R and Narita A 2020 Large-cavity coronoids with different inner and outer edge structures *J. Am. Chem. Soc.* **142** 12046–50

[54] Xu K *et al* 2019 On-surface synthesis of a nonplanar porous nanographene *J. Am. Chem. Soc.* **141** 7726–30

[55] Zeng Z *et al* 2022 Chemisorption-induced formation of biphenylene dimer on Ag(111) *J. Am. Chem. Soc.* **144** 723–32

[56] Zhang C, Kazuma E and Kim Y 2019 Atomic-scale visualization of the stepwise metal-mediated dehalogenative cycloaddition reaction pathways: competition between radicals and organometallic intermediates *Angew. Chem., Int. Ed.* **58** 17736–44

[57] Li Q, Gao J, Li Y, Fuentes-Cabrera M, Liu M, Qiu X, Lin H, Chi L and Pan M 2018 Self-assembly directed one-step synthesis of [4]radialene on Cu(100) surfaces *Nat. Commun.* **9** 3113

[58] Liu J *et al* 2019 Open-shell non-benzenoid nanographenes containing two pairs of pentagonal and heptagonal rings *J. Am. Chem. Soc.* **141** 12011–20

[59] Lohr T G *et al* 2020 On-surface synthesis of non-benzenoid nanographenes by oxidative ring-closure and ring-rearrangement reactions *J. Am. Chem. Soc.* **142** 13565–72

[60] Mallada B *et al* 2021 On-surface strain-driven synthesis of nonalternant non-benzenoid aromatic compounds containing four- to eight-membered rings *J. Am. Chem. Soc.* **143** 14694–702

[61] Stetsovych O, Švec M, Vacek J, Chocholoušová J V, Jančařík A, Rybáček J, Kosmider K, Stará I G, Jelínek P and Stary I 2017 From helical to planar chirality by on-surface chemistry *Nat. Chem.* **9** 213–8

[62] Bischoff F, Riss A, Michelitsch G S, Ducke J, Barth J V, Reuter K and Auwärter W 2021 Surface-mediated ring-opening and porphyrin deconstruction via conformational distortion *J. Am. Chem. Soc.* **143** 15131–8

[63] Kawai S *et al* 2016 Thermal control of sequential on-surface transformation of a hydrocarbon molecule on a copper surface *Nat. Commun.* **7** 12711

[64] Kawai S *et al* 2017 Competing annulene and radialene structures in a single anti-aromatic molecule studied by high-resolution atomic force microscopy *ACS Nano* **11** 8122–30

[65] Nakamura K, Li Q-Q, Krejčí O, Foster A S, Sun K, Kawai S and Ito S 2020 On-surface synthesis of a π-extended diaza[8]circulene *J. Am. Chem. Soc.* **142** 11363–9

[66] Mishra S, Fatayer S, Fernández S, Kaiser K, Peña D and Gross L 2022 Nonbenzenoid high-spin polycyclic hydrocarbons generated by atom manipulation *ACS Nano* **16** 3264–71

[67] Hieulle J, Carbonell-Sanromà E, Vilas-Varela M, Garcia-Lekue A, Guitián E, Peña D and Pascual J I 2018 On-surface route for producing planar nanographenes with azulene moieties *Nano Lett.* **18** 418–23

[68] Hou I C-Y, Sun Q, Eimre K, Di Giovannantonio M, Urgel J I, Ruffieux P, Narita A, Fasel R and Müllen K 2020 On-surface synthesis of unsaturated carbon nanostructures with regularly fused pentagon-heptagon pairs *J. Am. Chem. Soc.* **142** 10291–6

[69] Su J, Telychko M, Song S and Lu J 2020 Triangulenes: from precursor design to on-surface synthesis and characterization *Angew. Chem., Int. Ed.* **59** 7658–68

[70] Pavliček N, Mistry A, Majzik Z, Moll N, Meyer G, Fox D J and Gross L 2017 Synthesis and characterization of triangulene *Nat. Nanotechnol.* **12** 308–11

[71] Mishra S *et al* 2019 Synthesis and characterization of π-extended triangulene *J. Am. Chem. Soc.* **141** 10621–5

[72] Su J *et al* 2019 Atomically precise bottom-up synthesis of π-extended [5]triangulene *Sci. Adv.* **5** eaav7717

[73] Mishra S, Xu K, Eimre K, Komber H, Ma J, Pignedoli C A, Fasel R, Feng X and Ruffieux P 2021 Synthesis and characterization of [7]triangulene *Nanoscale* **13** 1624–8

[74] Su J *et al* 2021 On-surface synthesis and characterization of [7]triangulene quantum ring *Nano Lett.* **21** 861–7

[75] Mishra S *et al* 2020 Collective all-carbon magnetism in triangulene dimers *Angew. Chem., Int. Ed.* **59** 12041–7

[76] Cheng S, Xue Z, Li C, Liu Y, Xiang L, Ke Y, Yan K, Wang S and Yu P 2022 On-surface synthesis of triangulene trimers via dehydration reaction *Nat. Commun.* **13** 1705

[77] Mishra S *et al* 2021 Observation of fractional edge excitations in nanographene spin chains *Nature* **598** 287–92

[78] Wang T, Berdonces-Layunta A, Friedrich N, Vilas-Varela M, Calupitan J P, Pascual J I, Peña D, Casanova D, Corso M and de Oteyza D G 2022 Aza-triangulene: on-surface synthesis and electronic and magnetic properties *J. Am. Chem. Soc.* **144** 4522–9

[79] Hieulle J *et al* 2021 On-surface synthesis and collective spin excitations of a triangulene-based nanostar *Angew. Chem., Int. Ed.* **60** 25224–9

[80] Song S, Su J, Telychko M, Li J, Li G, Li Y, Su C, Wu J and Lu J 2021 On-surface synthesis of graphene nanostructures with π-magnetism *Chem. Soc. Rev.* **50** 3238–62

[81] Peng X *et al* 2021 Visualizing designer quantum states in stable macrocycle quantum corrals *Nat. Commun.* **12** 5895

[82] Labinger J A and Bercaw J E 2002 Understanding and exploiting C–H bond activation *Nature* **417** 507–14

[83] Kruppe C M, Krooswyk J D and Trenary M 2017 Selective hydrogenation of acetylene to ethylene in the presence of a carbonaceous surface layer on a Pd/Cu(111) single-atom alloy *ACS Catal.* **7** 8042–9

[84] Molina D L, Muir M, Abdel-Rahman M K and Trenary M 2021 The influence of palladium on the hydrogenation of acetylene on Ag(111) *J. Chem. Phys.* **154** 184701

[85] Shilov A E and Shul'pin G B 1997 Activation of C–H bonds by metal complexes *Chem. Rev.* **97** 2879–923

[86] Marcinkowski M D, Darby M T, Liu J, Wimble J M, Lucci F R, Lee S, Michaelides A, Flytzani-Stephanopoulos M, Stamatakis M and Sykes E C H 2018 Pt/Cu single-atom alloys as coke-resistant catalysts for efficient C–H activation *Nat. Chem.* **10** 325–32

[87] Rabe J P and Buchholz S 1991 Commensurability and mobility in two-dimensional molecular patterns on graphite *Science* **253** 424–7

[88] Askadskaya L and Rabe J P 1992 Anisotropic molecular dynamics in the vicinity of order-disorder transitions in organic monolayers *Phys. Rev. Lett.* **69** 1395–8

[89] Zhong D, Franke J-H, Podiyanachari S K, Blömker T, Zhang H, Kehr G, Erker G, Fuchs H and Chi L 2011 Linear alkane polymerization on a gold surface *Science* **334** 213–6

[90] Li Q *et al* 2016 Surface-controlled mono/diselective ortho C–H bond activation *J. Am. Chem. Soc.* **138** 2809–14

[91] Fan Q, Werner S, Tschakert J, Ebeling D, Schirmeisen A, Hilt G, Hieringer W and Gottfried J M 2018 Precise monoselective aromatic C–H bond activation by chemisorption of meta-aryne on a metal surface *J. Am. Chem. Soc.* **140** 7526–32

[92] Sun Q, Zhang C, Kong H, Tan Q and Xu W 2014 On-surface aryl-aryl coupling via selective C–H activation *Chem. Commun.* **50** 11825–8

[93] Zhang C, Sun Q, Chen H, Tan Q and Xu W 2015 Formation of polyphenyl chains through hierarchical reactions: Ullmann coupling followed by cross-dehydrogenative coupling *Chem. Commun.* **51** 495–8

[94] Hao Z *et al* 2022 Converting n-alkanol to conjugated polyenal on Cu(110) surface at mild temperature *J. Phys. Chem. Lett.* **13** 3276–82

[95] Li X *et al* 2021 Direct transformation of n-alkane into all-trans conjugated polyene via cascade dehydrogenation *Natl Sci. Rev.* **8** nwab093

[96] Hao Z *et al* 2022 From n-alkane to polyacetylene on Cu (110): linkage modulation in chain growth *Sci. China Chem.* **65** 733–9

[97] Guo W *et al* 2022 Visualization of on-surface ethylene polymerization through ethylene insertion *Science* **375** 1188–91

[98] Okawa Y and Aono M 2001 Nanoscale control of chain polymerization *Nature* **409** 683–4

[99] Okawa Y and Aono M 2001 Linear chain polymerization initiated by a scanning tunneling microscope tip at designated positions *J. Chem. Phys.* **115** 2317–22

[100] Miura A, De Feyter S, Abdel-Mottaleb M M S, Gesquière A, Grim P C M, Moessner G, Sieffert M, Klapper M, Müllen K and De Schryver F C 2003 Light- and STM-tip-induced formation of one-dimensional and two-dimensional organic nanostructures *Langmuir* **19** 6474–82

[101] Sun Q *et al* 2016 Bottom-up synthesis of metalated carbyne *J. Am. Chem. Soc.* **138** 1106–9

[102] Yu X, Li X, Lin H, Liu M, Cai L, Qiu X, Yang D, Fan X, Qiu X and Xu W 2020 Bond-scission-induced structural transformation from cumulene to diyne moiety and formation of semiconducting organometallic polyyne *J. Am. Chem. Soc.* **142** 8085–9

[103] Gao W, Kang F, Qiu X, Yi Z, Shang L, Liu M, Qiu X, Luo Y and Xu W 2022 On-surface debromination of $C_6Br_6$: $C_6$ ring versus $C_6$ chain *ACS Nano* **16** 6578–84

[104] Yu X *et al* 2022 Lattice-directed selective synthesis of acetylenic and diacetylenic organometallic polyynes *Chem. Mater.* **34** 1770–7

[105] Wang S *et al* 2019 On-surface synthesis and characterization of individual polyacetylene chains *Nat. Chem.* **11** 924–30

[106] Wang C, Batsanov A S, Bryce M R, Martín S, Nichols R J, Higgins S J, García-Suárez V M and Lambert C J 2009 Oligoyne single molecule wires *J. Am. Chem. Soc.* **131** 15647–54

[107] Pavliček N, Schuler B, Collazos S, Moll N, Pérez D, Guitián E, Meyer G, Peña D and Gross L 2015 On-surface generation and imaging of arynes by atomic force microscopy *Nat. Chem.* **7** 623–8

[108] Schuler B, Fatayer S, Mohn F, Moll N, Pavliček N, Meyer G, Peña D and Gross L 2016 Reversible Bergman cyclization by atomic manipulation *Nat. Chem.* **8** 220–4

[109] Pavliček N, Majzik Z, Collazos S, Meyer G, Pérez D, Guitián E, Peña D and Gross L 2017 Generation and characterization of a meta-aryne on Cu and NaCl surfaces *ACS Nano* **11** 10768–73

[110] de Oteyza D G *et al* 2013 Direct imaging of covalent bond structure in single-molecule chemical reactions *Science* **340** 1434–7

[111] Repp J, Meyer G, Stojković S M, Gourdon A and Joachim C 2005 Molecules on insulating films: scanning-tunneling microscopy imaging of individual molecular orbitals *Phys. Rev. Lett.* **94** 26803

[112] Albrecht F, Rey D, Fatayer S, Schulz F, Pérez D, Peña D and Gross L 2020 Intramolecular coupling of terminal alkynes by atom manipulation *Angew. Chem., Int. Ed.* **59** 22989–93

[113] Repp J, Meyer G, Paavilainen S, Olsson F E and Persson M 2006 Imaging bond formation between a gold atom and pentacene on an insulating surface *Science* **312** 1196–9

[114] Liljeroth P, Repp J and Meyer G 2007 Current-induced hydrogen tautomerization and conductance switching of naphthalocyanine molecules *Science* **317** 1203–6

[115] Morgenstern K, Lorente N and Rieder K-H 2013 Controlled manipulation of single atoms and small molecules using the scanning tunnelling microscope *Phys. Status Solidi* b **250** 1671–751

[116] Hla S-W, Bartels L, Meyer G and Rieder K-H 2000 Inducing all steps of a chemical reaction with the scanning tunneling microscope tip: towards single molecule engineering *Phys. Rev. Lett.* **85** 2777–80

[117] Zhong Q, Ihle A, Ahles S, Wegner H A, Schirmeisen A and Ebeling D 2021 Constructing covalent organic nanoarchitectures molecule by molecule via scanning probe manipulation *Nat. Chem.* **13** 1133–9

[118] Rizzo D J, Veber G, Jiang J, McCurdy R, Cao T, Bronner C, Chen T, Louie S G, Fischer F R and Crommie M F 2020 Inducing metallicity in graphene nanoribbons via zero-mode superlattices *Science* **369** 1597–603

[119] Fan Q *et al* 2021 Biphenylene network: a nonbenzenoid carbon allotrope *Science* **372** 852–6

[120] Blackwell R E, Zhao F, Brooks E, Zhu J, Piskun I, Wang S, Delgado A, Lee Y-L, Louie S G and Fischer F R 2021 Spin splitting of dopant edge state in magnetic zigzag graphene nanoribbons *Nature* **600** 647–52

[121] Wang T *et al* 2022 Magnetic interactions between radical pairs in chiral graphene nanoribbons *Nano Lett.* **22** 164–71

[122] Yang L, Park C-H, Son Y-W, Cohen M L and Louie S G 2007 Quasiparticle energies and band gaps in graphene nanoribbons *Phys. Rev. Lett.* **99** 186801

[123] Talirz L, Ruffieux P and Fasel R 2016 On-surface synthesis of atomically precise graphene nanoribbons *Adv. Mater.* **28** 6222–31

[124] Cai J *et al* 2010 Atomically precise bottom-up fabrication of graphene nanoribbons *Nature* **466** 470–3

[125] Ruffieux P *et al* 2016 On-surface synthesis of graphene nanoribbons with zigzag edge topology *Nature* **531** 489–92

[126] Berdonces-Layunta A, Schulz F, Aguilar-Galindo F, Lawrence J, Mohammed M S G, Muntwiler M, Lobo-Checa J, Liljeroth P and de Oteyza D G 2021 Order from a mess: the growth of 5-armchair graphene nanoribbons *ACS Nano* **15** 16552–61

[127] Sánchez-Sánchez C, Dienel T, Deniz O, Ruffieux P, Berger R, Feng X, Müllen K and Fasel R 2016 Purely armchair or partially chiral: noncontact atomic force microscopy

characterization of dibromo-bianthryl-based graphene nanoribbons grown on Cu(111) *ACS Nano* **10** 8006–11
[128] de Oteyza D G *et al* 2016 Substrate-independent growth of atomically precise chiral graphene nanoribbons *ACS Nano* **10** 9000–8
[129] Cai J *et al* 2014 Graphene nanoribbon heterojunctions *Nat. Nanotechnol.* **9** 896–900
[130] Kawai S, Saito S, Osumi S, Yamaguchi S, Foster A S, Spijker P and Meyer E 2015 Atomically controlled substitutional boron-doping of graphene nanoribbons *Nat. Commun.* **6** 8098
[131] Zhang Y *et al* 2022 On-surface synthesis of a nitrogen-doped graphene nanoribbon with multiple substitutional sites *Angew. Chem., Int. Ed.* **61** e202204736
[132] Moreno C *et al* 2018 Bottom-up synthesis of multifunctional nanoporous graphene *Science* **360** 199–203
[133] Tenorio M, Moreno C, Febrer P, Castro-esteban J, Ordejón P, Peña D, Pruneda M and Mugarza A 2022 Atomically sharp lateral superlattice heterojunctions built-in nitrogen-doped nanoporous graphene *Adv. Mater.* **34** e2110099
[134] Chen Y-C, de Oteyza D G, Pedramrazi Z, Chen C, Fischer F R and Crommie M F 2013 Tuning the band gap of graphene nanoribbons synthesized from molecular precursors *ACS Nano* **7** 6123–8
[135] Talirz L *et al* 2017 On-surface synthesis and characterization of 9-atom wide armchair graphene nanoribbons *ACS Nano* **11** 1380–8
[136] Ruffieux P *et al* 2012 Electronic structure of atomically precise graphene nanoribbons *ACS Nano* **6** 6930–5
[137] Rizzo D J, Veber G, Cao T, Bronner C, Chen T, Zhao F, Rodriguez H, Louie S G, Crommie M F and Fischer F R 2018 Topological band engineering of graphene nanoribbons *Nature* **560** 204–8
[138] Gröning O *et al* 2018 Engineering of robust topological quantum phases in graphene nanoribbons *Nature* **560** 209–13
[139] Cao T, Zhao F and Louie S G 2017 Topological phases in graphene nanoribbons: junction states, spin centers, and quantum spin chains *Phys. Rev. Lett.* **119** 76401
[140] Rizzo D J *et al* 2021 Rationally designed topological quantum dots in bottom-up graphene nanoribbons *ACS Nano* **15** 20633–42
[141] Li S, Liu M and Qiu X 2020 Scanning probe microscopy of topological structure induced electronic states of graphene *Small Methods* **4** 1900683
[142] Liu M *et al* 2017 Graphene-like nanoribbons periodically embedded with four- and eight-membered rings *Nat. Commun.* **8** 14924
[143] Liu M, Liu M, Zha Z, Pan J, Qiu X, Li T, Wang J, Zheng Y and Zhong D 2018 Thermally induced transformation of nonhexagonal carbon rings in graphene-like nanoribbons *J. Phys. Chem.* C **122** 9586–92
[144] Li D-Y *et al* 2021 Ladder phenylenes synthesized on Au(111) surface via selective [2+2] cycloaddition *J. Am. Chem. Soc.* **143** 12955–60
[145] Fan Q, Martin-Jimenez D, Ebeling D, Krug C K, Brechmann L, Kohlmeyer C, Hilt G, Hieringer W, Schirmeisen A and Gottfried J M 2019 Nanoribbons with nonalternant topology from fusion of polyazulene: carbon allotropes beyond graphene *J. Am. Chem. Soc.* **141** 17713–20
[146] de la Torre B *et al* 2020 Tailoring π-conjugation and vibrational modes to steer on-surface synthesis of pentalene-bridged ladder polymers *Nat. Commun.* **11** 4567
[147] Di Giovannantonio M, Urgel J I, Beser U, Yakutovich A V, Wilhelm J, Pignedoli C A, Ruffieux P, Narita A, Müllen K and Fasel R 2018 On-surface synthesis of indenofluorene polymers by oxidative five-membered ring formation *J. Am. Chem. Soc.* **140** 3532–6
[148] Sun Q *et al* 2018 Direct formation of C–C triple-bonded structural motifs by on-surface dehalogenative homocouplings of tribromomethyl-substituted arenes *Angew. Chem., Int. Ed.* **57** 4035–8
[149] Sánchez-Grande A *et al* 2019 On-surface synthesis of ethynylene-bridged anthracene polymers *Angew. Chem., Int. Ed.* **58** 6559–63
[150] Sun K, Sagisaka K, Peng L, Watanabe H, Xu F, Pawlak R, Meyer E, Okuda Y, Orita A and Kawai S 2021 Head-to-tail oligomerization by silylene-tethered Sonogashira coupling on Ag(111) *Angew. Chem., Int. Ed.* **60** 19598–603
[151] Kawai S *et al* 2022 On-surface synthesis of porphyrin-complex multi-block co-oligomers by defluorinative coupling *Angew. Chem., Int. Ed.* **61** e202114697
[152] Sun Q, Cai L, Ma H, Yuan C and Xu W 2016 Dehalogenative homocoupling of terminal alkynyl bromides on Au(111): incorporation of acetylenic scaffolding into surface nanostructures *ACS Nano* **10** 7023–30
[153] Kawai S, Krejčí O, Foster A S, Pawlak R, Xu F, Peng L, Orita A and Meyer E 2018 Diacetylene linked anthracene oligomers synthesized by one-shot homocoupling of trimethylsilyl on Cu(111) *ACS Nano* **12** 8791–7
[154] Sánchez-Grande A *et al* 2020 Diradical organic one-dimensional polymers synthesized on a metallic surface *Angew. Chem., Int. Ed.* **59** 17594–9
[155] Zhang C, Jaculbia R B, Tanaka Y, Kazuma E, Imada H, Hayazawa N, Muranaka A, Uchiyama M and Kim Y 2021 Chemical identification and bond control of π-skeletons in a coupling reaction *J. Am. Chem. Soc.* **143** 9461–7
[156] Urgel J I *et al* 2020 On-surface synthesis of cumulene-containing polymers via two-step dehalogenative homocoupling of dibromomethylene-functionalized tribenzoazulene *Angew. Chem., Int. Ed.* **59** 13281–7
[157] Cirera B *et al* 2020 Tailoring topological order and π-conjugation to engineer quasi-metallic polymers *Nat. Nanotechnol.* **15** 437–43
[158] Zhong Q, Niu K, Chen L, Zhang H, Ebeling D, Björk J, Müllen K, Schirmeisen A and Chi L 2022 Substrate-modulated synthesis of metal-organic hybrids by tunable multiple aryl-metal bonds *J. Am. Chem. Soc.* **144** 8214–22
[159] Fan Q, Wang T, Dai J, Kuttner J, Hilt G, Gottfried J M and Zhu J 2017 On-surface pseudo-high-dilution synthesis of macrocycles: principle and mechanism *ACS Nano* **11** 5070–9
[160] Kolmer M, Zuzak R, Steiner A K, Zajac L, Engelund M, Godlewski S, Szymonski M and Amsharov K 2019 Fluorine-programmed nanozipping to tailored nanographenes on rutile $TiO_2$ surfaces *Science* **363** 57–60
[161] Zhan G, Cai Z-F, Strutyński K, Yu L, Herrmann N, Martínez-Abadía M, Melle-Franco M, Mateo-Alonso A and De Feyter S 2022 Observing polymerization in 2D dynamic covalent polymers *Nature* **603** 835–40
[162] Lu C, Mo Y-P, Hong Y, Chen T, Yang Z-Y, Wan L-J and Wang D 2020 On-surface growth of single-layered homochiral 2D covalent organic frameworks by steric hindrance strategy *J. Am. Chem. Soc.* **142** 14350–6
[163] Liu X-H, Guan C-Z, Ding S-Y, Wang W, Yan H-J, Wang D and Wan L-J 2013 On-surface synthesis of single-layered two-dimensional covalent organic frameworks via solid-vapor interface reactions *J. Am. Chem. Soc.* **135** 10470–4
[164] Dienstmaier J F, Medina D D, Dogru M, Knochel P, Bein T, Heckl W M and Lackinger M 2012 Isoreticular two-dimensional covalent organic frameworks synthesized by on-surface condensation of diboronic acids *ACS Nano* **6** 7234–42

[165] Liu X-H, Guan C-Z, Wang D and Wan L-J 2014 Graphene-like single-layered covalent organic frameworks: synthesis strategies and application prospects *Adv. Mater.* **26** 6912–20
[166] Zhang R *et al* 2013 Chemical mapping of a single molecule by plasmon-enhanced Raman scattering *Nature* **498** 82–86
[167] Wang R-P *et al* 2021 Raman detection of bond breaking and making of a chemisorbed up-standing single molecule at single-bond level *J. Phys. Chem. Lett.* **12** 1961–8
[168] Xu J *et al* 2021 Determining structural and chemical heterogeneities of surface species at the single-bond limit *Science* **371** 818–22
[169] Kazuma E, Jung J, Ueba H, Trenary M and Kim Y 2017 Direct pathway to molecular photodissociation on metal surfaces using visible light *J. Am. Chem. Soc.* **139** 3115–21
[170] Yu M *et al* 2020 Long-range ordered and atomic-scale control of graphene hybridization by photocycloaddition *Nat. Chem.* **12** 1035–41
[171] Nacci C, Baroncini M, Credi A and Grill L 2018 Reversible photoswitching and isomer-dependent diffusion of single azobenzene tetramers on a metal surface *Angew. Chem., Int. Ed.* **57** 15034–9
[172] Galanti A, Diez-Cabanes V, Santoro J, Valášek M, Minoia A, Mayor M, Cornil J and Samorì P 2018 Electronic decoupling in $C_3$-symmetrical light-responsive tris(azobenzene) scaffolds: self-assembly and multiphotochromism *J. Am. Chem. Soc.* **140** 16062–70
[173] Zhang X, Xu S, Li M, Shen Y, Wei Z, Wang S, Zeng Q and Wang C 2012 Photo-induced polymerization and isomerization on the surface observed by scanning tunneling microscopy *J. Phys. Chem.* C **116** 8950–5
[174] Kazuma E, Jung J, Ueba H, Trenary M and Kim Y 2018 Real-space and real-time observation of a plasmon-induced chemical reaction of a single molecule *Science* **360** 521–6
[175] Kazuma E, Lee M, Jung J, Trenary M and Kim Y 2020 Single-molecule study of a plasmon-induced reaction for a strongly chemisorbed molecule *Angew. Chem., Int. Ed.* **59** 7960–6
[176] Böckmann H, Gawinkowski S, Waluk J, Raschke M B, Wolf M and Kumagai T 2018 Near-field enhanced photochemistry of single molecules in a scanning tunneling microscope junction *Nano Lett.* **18** 152–7
[177] Mahapatra S, Schultz J F, Li L, Zhang X and Jiang N 2022 Controlling localized plasmons via an atomistic approach: attainment of site-selective activation inside a single molecule *J. Am. Chem. Soc.* **144** 2051–5
[178] Tanaka H and Kawai T 2009 Partial sequencing of a single DNA molecule with a scanning tunnelling microscope *Nat. Nanotechnol.* **4** 518–22
[179] Saywell A, Sprafke J K, Esdaile L J, Britton A J, Rienzo A, Anderson H L, O'Shea J N and Beton P H 2010 Conformation and packing of porphyrin polymer chains deposited using electrospray on a gold surface *Angew. Chem., Int. Ed.* **49** 9136–9
[180] O'Sullivan M C *et al* 2011 Vernier templating and synthesis of a 12-porphyrin nano-ring *Nature* **469** 72–75
[181] McCurdy R D, Jacobse P H, Piskun I, Veber G C, Rizzo D J, Zuzak R, Mutlu Z, Bokor J, Crommie M F and Fischer F R 2021 Synergetic bottom-up synthesis of graphene nanoribbons by matrix-assisted direct transfer *J. Am. Chem. Soc.* **143** 4174–8
[182] Loth S, Etzkorn M, Lutz C P, Eigler D M and Heinrich A J 2010 Measurement of fast electron spin relaxation times with atomic resolution *Science* **329** 1628–30
[183] Terada Y, Yoshida S, Takeuchi O and Shigekawa H 2010 Real-space imaging of transient carrier dynamics by nanoscale pump–probe microscopy *Nat. Photon.* **4** 869–74
[184] Cocker T L, Peller D, Yu P, Repp J and Huber R 2016 Tracking the ultrafast motion of a single molecule by femtosecond orbital imaging *Nature* **539** 263–7
[185] Wiesendanger R, Güntherodt H, Güntherodt G, Gambino R J and Ruf R 1990 Observation of vacuum tunneling of spin-polarized electrons with the scanning tunneling microscope *Phys. Rev. Lett.* **65** 247–50
[186] Wiesendanger R 2009 Spin mapping at the nanoscale and atomic scale *Rev. Mod. Phys.* **81** 1495–550
[187] Yamamoto S, Imada H and Kim Y 2022 Atomic-scale photon mapping revealing spin-current relaxation *Phys. Rev. Lett.* **128** 206804
[188] Zhong J-H, Jin X, Meng L, Wang X, Su H-S, Yang Z-L, Williams C T and Ren B 2017 Probing the electronic and catalytic properties of a bimetallic surface with 3 nm resolution *Nat. Nanotechnol.* **12** 132–6
[189] Lee J, Crampton K T, Tallarida N and Apkarian V A 2019 Visualizing vibrational normal modes of a single molecule with atomically confined light *Nature* **568** 78–82
[190] Jaculbia R B, Imada H, Miwa K, Iwasa T, Takenaka M, Yang B, Kazuma E, Hayazawa N, Taketsugu T and Kim Y 2020 Single-molecule resonance Raman effect in a plasmonic nanocavity *Nat. Nanotechnol.* **15** 105–10
[191] Yin H *et al* 2020 Nanometre-scale spectroscopic visualization of catalytic sites during a hydrogenation reaction on a Pd/Au bimetallic catalyst *Nat. Catal.* **3** 834–42
[192] Schultz J F, Li S, Jiang S and Jiang N 2020 Optical scanning tunneling microscopy based chemical imaging and spectroscopy *J. Phys.: Condens. Matter* **32** 463001
[193] Nonnenmacher M, O'Boyle M P and Wickramasinghe H K 1991 Kelvin probe force microscopy *Appl. Phys. Lett.* **58** 2921–3
[194] Castañeda-Uribe O A, Reifenberger R, Raman A and Avila A 2015 Depth-sensitive subsurface imaging of polymer nanocomposites using second harmonic Kelvin probe force microscopy *ACS Nano* **9** 2938–47